Equilibria, Stability, and Sensitivity for the Aerial Suspended Beam Robotic System Subject to Parameter Uncertainty

Chiara Gabellieri, *Member, IEEE*, Marco Tognon, *Member, IEEE*, Dario Sanalitro, and Antonio Franchi, *Fellow, IEEE*

***Abstract*—This article studies how parametric uncertainties affect the cooperative manipulation of a cable-suspended beam-shaped load by means of two aerial robots not explicitly communicating with each other. In particular, this article sheds light on the impact of the uncertain knowledge of the model parameters available to an established communicationless force-based controller. First, we find the closed-loop equilibrium configurations in the presence of the aforementioned uncertainties, and then, we study their stability. Hence, we show the fundamental role played in the robustness of the load attitude control by the internal force induced in the manipulated object by nonvertical cables. Furthermore, we formally study the sensitivity of the attitude error to such parametric variations, and we provide a method to act on the load position error in the presence of uncertainties. Eventually, we validate the results through an extensive set of numerical tests in a realistic simulation environment, including underactuated aerial vehicles and sagging-prone cables, and through hardware experiments.**

***Index Terms*—Aerial systems, cooperative aerial manipulation, mechanics and control, motion control.**

Manuscript received 1 March 2023; accepted 12 May 2023. Date of publication 13 June 2023; date of current version 4 October 2023. This work was supported in part by the European Union's Horizon Europe Research and Innovation Program "Flyflic" under Grant 101059875 and Horizon 2020 Research and Innovation Program "AERIAL-CORE" under Grant 871479. This paper was recommended for publication by Associate Editor H. G. de Marina and Editor P. R. Giordano upon evaluation of the reviewers' comments. *(Corresponding author: Chiara Gabellieri.)*

Chiara Gabellieri is with the Robotics and Mechatronics Group, Faculty of Electrical Engineering, Mathematics and Computer Science, University of Twente, 7500 AE Enschede, The Netherlands (e-mail: c.gabellieri@utwente.nl).

Marco Tognon is with the Univ Rennes, CNRS, Inria, IRISA, F-35000 Rennes, France (e-mail: marco.tognon@inria.fr).

Dario Sanalitro was with the Laboratory for Analysis and Architecture of Systems, French National Center for Scientific Research, University of Toulouse, 31400 Toulouse, France. He is now with the Electrical electronic and computer engineering department, University of Catania, 95125 Catania, Italy (e-mail: dario.sanalitro@laas.fr).

Antonio Franchi is with the Robotics and Mechatronics Group, Faculty of Electrical Engineering, Mathematics and Computer Science, University of Twente, 7500 AE Enschede, The Netherlands, also with the Department of Computer, Control and Management Engineering, Sapienza University of Rome, 00185 Rome, Italy, and also with LAAS-CNRS, Université de Toulouse, CNRS, Toulouse, France (e-mail: a.franchi@utwente.nl).

This article has supplementary material provided by the authors and color versions of one or more figures available at https://doi.org/10.1109/TRO.2023.3279033.

Digital Object Identifier 10.1109/TRO.2023.3279033

I. Introduction

IT IS nowadays acknowledged that the interest in unmanned aerial vehicles (UAVs) is becoming wider and wider by virtue of their ability to embrace an ample set of applications. A very recent and popular topic in aerial robotics is physical interaction using aerial manipulators [1], [2], [3] for applications such as contact-based inspection, assembly, human assistance, etc. To solve these challenges, aerial platforms are endowed with physical interaction tools, such as cables [4] or more complex robotic arms [5].

Researchers have considered taking advantage of the cooperation between multiple robots to enhance the overall payload and manipulate large objects [6], [7], [8], [9]. Different methods have been developed to tackle multirobot aerial manipulation. Nguyen et al. [10] and Ritz and D'Andrea [11] use passive manipulation tools to solve the cooperative aerial transportation of rigid and elastic objects, respectively. Multiple flying arms are instead used in [12] and [13]. Cables have been often considered in multirobot manipulation scenarios, because, in addition to being lightweight and low cost, they also mitigate the coupling between the system dynamics and the robots' attitude, which can simplify the control problem, especially when using underactuated aerial platforms.

A. Related Works

The problem of manipulating a cable-suspended load through a team of aerial vehicles has been studied, e.g., in [14], [15], [16], [17], [18], and [19]. In [20], a robust pose controller for a cable-suspended load manipulated by multiple UAVs is presented. Stability is ensured through gain tuning given a bound on the uncertainties affecting the kinematic parameters. Formation control to transport the payload with a focus on robustness is described in [21], where modeling uncertainties are also taken into account.

A standard system that has attracted substantial interest in the research community is composed of two aerial vehicles manipulating a *beam-like load* through cables [17], [22], [23], [24], [25], [26], [27]. Such standard configuration is of interest for several real-world applications, especially in the construction field, where we find columns, wooden pillars, iron beams for cement walls, scaffolds, pipes, pieces of roofs, and other beam-like building elements. Two is the minimum number of

aerial robots allowing to control both the position and attitude of a cable-suspended beam-like load [23]. While three aerial robots allow controlling the entire pose of a generic rigid body [28], using more than two robots for a beam-like load, it is arguably not the optimal solution in most of the cases because of the increased complexity of the system without being necessary for the control of the load.

Pereira and Dimarogonas [23] and Goodman and Colombo [29] propose a method for the transportation of a cable-suspended beam load by two aerial vehicles that have access to the state of the load; they consider rigid and elastic cables, respectively. In [24], centralized and decentralized model-predictive control is proposed for a system of two UAVs manipulating a beam load through cables.

Decentralized algorithms as [30] are more robust and scalable with respect to (w.r.t.) the number of robots. However, decentralized *communicationless* approaches have also been intensively studied in the literature [31] because communication delays and packet losses are among the principal causes undermining the performance and stability of the system in real implementations, and because the hardware and software complexity can be reduced by confining explicit communication. In [26], a method relying on visual feedback is presented. As an alternative to vision, a force-based method that uses admittance controllers and a leader–follower scheme is typically used to address communicationless aerial manipulation of cable-suspended objects [25], [32], [33], [34]. The leader robot guides the system following a predetermined trajectory, while the second robot, which carries a portion of the load weight, follows its lead by sensing the cable force variations.

A primary goal of [25] is to keep the cables always vertical during transportation, meaning that no internal force is induced in the object. Tagliabue et al. [32] extend the results of [25] toward the N-robot case and provide a method for tuning the gains of the admittance controllers to improve the robustness against unmodeled dynamics and parametric uncertainties. In both the works, experiments are shown, in which, however, the altitude of the robots is set to a predetermined reference, implying either a centralized vertical movement coordination or restricted vertical motion.

For such a popular class of communicationless, admittance-controlled, and leader–follower schemes, the formal analysis of the closed-loop system equilibrium configurations and their stability was presented for the first time in our previous work [33]. There, we showed that inducing an internal force on the load through nonvertical cables is required for full-pose regulation, especially to prevent arbitrary vertical movements of the robots that would interfere with the regulation of the load pitch and center position. In [34], we considered N robots, empirically showing through extensive simulations the effect of changing the number of leader robots on the stability and robustness against disturbances. Both the works tackle only the ideal case, where perfect knowledge of the system parameters is available to the admittance controllers of each aerial robot.

Despite being of primary interest, it has been unclear until now if and how in-practice-unavoidable uncertainties impact the pose regulation in the aforementioned control framework. Such a gap is filled in this article by introducing uncertainties on those system parameters used in the control action.

Adaptive control laws have been proposed in the literature for the system in question; however, they are based on different assumptions than those used in this article. For instance, the full state has been considered available for feedback in [31], or the robots rigidly attached to the object [35], [36]. Other works assume that the load mass is the sole uncertain parameter and only focuses on the translational velocity regulation [13], or relies on a communication network [37].

In this article, we have found that the internal force induced by nonvertical cables plays a fundamental role in enabling task execution, especially in realistic conditions characterized by uncertainties. The importance of this is masked when vertical movements of the robots are prevented or the leader–follower approach is used solely to regulate the load motion in the horizontal plane, as in [25] and [32]. On the other hand, the role of the internal force is crucial if the admittance-based communicationless approach is applied in the full 3-D space, and hence, communicationless full-pose regulation is sought.

While some loads may be damaged by internal forces, this is easily prevented, in practice, by enclosing the loads in suitable cases. In addition, internal forces require additional control effort, which is justified by the benefits in terms of convergence and robustness of the load pose control, as will be clear in the following. Indeed, internal forces have been often proposed also in the robotic grasping literature as a tool to make the grip on the object robust thanks to friction [38].

B. Contributions and Outline of This Article

The contribution of this article is showing the effects of parametric uncertainties on the static regulation of the load pose when the usual approach [25], [32], [33], [34] based on admittance-controlled leader–follower aerial robots is used for manipulating a cable-suspended beam in the absence of explicit communication. In this approach, each robot knows only its own state and the force in its cable, retrievable from the robot's state using an external force observer.

Note that, unlike in [29], it is not feasible to assume that all the robots have knowledge of the object state. This is because the object state is based on the state of all the robots, but data exchange among them is not considered in our scenario. Throughout this article, we show that it is best to avoid the intuitive idea of having the cables vertical when performing the manipulation with force-based methods in real scenarios, i.e., when uncertainties are present. We address the problem aiming at a mathematically sound point of view. We point out that we restrict the analysis to pose *regulation*, hence, to quasi-static motion of the load. Tracking of more aggressive trajectories is left to future work. With the above context in mind, the key contributions can be succinctly summarized.

1) After formally studying the equilibrium points of the closed-loop system in the presence of uncertain parameters, their stability is proved using Lyapunov's theory.

TABLE I
NOTATION—GENERAL SYMBOLS AND REFERENCE FRAMES

$\boldsymbol{I}_i$	$i \times i$ identity matrix
$\boldsymbol{e}_i$	ith column of $\boldsymbol{I}_3$
$\boldsymbol{S}(\star)$	skew operator
$Ker(\star)$	nullspace of $\star$
diag($\star$)	diagonal matrix
$\star^\top$	transpose of $\star$
$\|\star\|$	2-norm of $\star$
$\bar{\star}$	desired value of $\star$
$\star^{\text{Eq}}$	value of $\star$ at the equilibrium
$\hat{\star}$	uncertain value of $\star$
$\Delta_\star$	$\star - \hat{\star}$
$\mathcal{F}_W$	inertial reference frame
$\mathcal{F}_L$	load reference frame
$\mathcal{F}_{Ri}$	ith robot reference frame
$\{O_A, \boldsymbol{x}_A, \boldsymbol{y}_A, \boldsymbol{z}_A\}$	Origin, x-axis, y-axis, and z-axis of $\mathcal{F}_A$
${}^L\star$	$\star$ expressed in $\mathcal{F}_L$
$\dot{\star}$	time derivative of $\star$

TABLE II
NOTATION—SYSTEM VARIABLES

g	gravity acceleration
$\boldsymbol{p}_L, \dot{\boldsymbol{p}}_L, \ddot{\boldsymbol{p}}_L$	load position, velocity, acceleration
$\boldsymbol{R}_L$	rotation of $\mathcal{F}_L$ w.r.t. $\mathcal{F}_W$
$\boldsymbol{\omega}_L$	load angular velocity
$\boldsymbol{q}_L$	set composed of $(\boldsymbol{p}_L, \boldsymbol{R}_L)$
$\boldsymbol{v}_L$	$[\dot{\boldsymbol{p}}_L^\top \ {}^L\boldsymbol{\omega}_L^\top]^\top$
ψ, θ	yaw and pitch of the load
B_i	ith cable attaching point on load
$\boldsymbol{b}_1$	position of point B_i
m_L, $\boldsymbol{J}_L$	load mass and rotational inertia
L	load length, with $\ell = 1/L$
$\boldsymbol{M}_L$	diag($m_L \boldsymbol{I}_3, \boldsymbol{J}_L$)
$\boldsymbol{g}_L$	gravity terms in load dynamics
$\boldsymbol{c}_L$	Coriolis terms in load dynamics
$\boldsymbol{G}$	load grasp matrix
$\boldsymbol{p}_{Ri}, \dot{\boldsymbol{p}}_{Ri}, \ddot{\boldsymbol{p}}_{Ri}$	ith robot position, velocity, acceleration
$\boldsymbol{R}_{Ri}$	rotation of $\mathcal{F}_{Ri}$ w.r.t. $\mathcal{F}_W$
$\boldsymbol{q}_R$	$[\boldsymbol{p}_{R1}^\top \ \boldsymbol{p}_{R2}^\top]^\top$
k_i	stiffness of the ith cable
l_{0i}	rest length of the ith cable
$\boldsymbol{l}_i$	$\boldsymbol{p}_{Ri} - \boldsymbol{b}_i$, vector along the ith cable
$\boldsymbol{f}_i$	force of the ith cable on the load
$\boldsymbol{f}$	$[\boldsymbol{f}_1^\top \ \boldsymbol{f}_2^\top]^\top$
$\boldsymbol{q}$	set $(\boldsymbol{q}_R, \boldsymbol{q}_R)$
$\boldsymbol{v}$	$[\boldsymbol{v}_R^\top \ \boldsymbol{v}_L^\top]^\top$
$\boldsymbol{x}$	$(\boldsymbol{q}, \boldsymbol{v})$
$\boldsymbol{u}_{Ri}$	control input of robot ith
$\boldsymbol{M}_{Ai}$	ith robot control gain: apparent inertia, $\boldsymbol{M}_A$ diag($\boldsymbol{M}_{A1}, \boldsymbol{M}_{A2}$)
$\boldsymbol{B}_{Ai}$	ith robot control gain: apparent damping, $\boldsymbol{B}_A$ diag($\boldsymbol{B}_{A1}, \boldsymbol{B}_{A2}$)
$\boldsymbol{K}_{Ai}$	ith robot control gain: virtual spring stiffness, $\boldsymbol{K}_A$ diag($\boldsymbol{K}_{A1}, \boldsymbol{K}_{A2}$)
$\boldsymbol{\pi}_{Ai}$	feedforward term of ith robot's control, $\boldsymbol{\pi}_A = [\boldsymbol{\pi}_{A1}^\top \ \boldsymbol{\pi}_{A2}^\top]^\top$
t_L	load internal force
ξ	$\left(b_1 m_L - \frac{\hat{b}_1 \hat{m}_L L}{\hat{L}}\right)$
$m(\boldsymbol{q}, \boldsymbol{v}, \boldsymbol{\pi}_A)$	closed-loop dynamics
$\mathcal{Q}(t_L, \bar{\boldsymbol{q}}_L)$	$\{\boldsymbol{q}$ satisfying Theorem 2$\}$
$\mathcal{Q}^+(t_L, \bar{\boldsymbol{q}}_L)$	$\mathcal{Q}(t_L, \bar{\boldsymbol{q}}_L)$ where $\boldsymbol{R}_L^{eq}\boldsymbol{e}_1$ has same sign of (17)
$\boldsymbol{R}_L^{eq+}$	$\boldsymbol{R}_L^{eq}$ in $\boldsymbol{q} \in \mathcal{Q}^+(t_L, \bar{\boldsymbol{q}}_L)$
$\boldsymbol{R}_L^{eq-}$	$\boldsymbol{R}_L^{eq+}\boldsymbol{R}_{\boldsymbol{z}_L}(\pi)$
$\mathcal{Q}^-(t_L, \bar{\boldsymbol{q}}_L)$	$\boldsymbol{q} \in \mathcal{Q}(t_L, \bar{\boldsymbol{q}}_L)$ s.t. $\boldsymbol{R}_L^{eq} = \boldsymbol{R}_L^{eq-}$
$\mathcal{Q}_1(0, \bar{\boldsymbol{q}}_L)$	$\boldsymbol{q} \in \mathcal{Q}(0, \bar{\boldsymbol{q}}_L)$ s.t. $(\boldsymbol{R}_L^{eq}\boldsymbol{e}_1)^\top \boldsymbol{e}_3 = +1$
$\mathcal{Q}_2(0, \bar{\boldsymbol{q}}_L)$	$\boldsymbol{q} \in \mathcal{Q}(0, \bar{\boldsymbol{q}}_L)$ s.t. $(\boldsymbol{R}_L^{eq}\boldsymbol{e}_1)^\top \boldsymbol{e}_3 = -1$
$\mathcal{X}(0, \bar{\boldsymbol{q}}_L)$	$\{\boldsymbol{x} : \boldsymbol{q} \in \mathcal{Q}(0, \bar{\boldsymbol{q}}_L), \boldsymbol{v} = \boldsymbol{0}\}$
$\mathcal{X}_i(0, \bar{\boldsymbol{q}}_L)$	$\{\boldsymbol{x} : \boldsymbol{q} \in \mathcal{Q}_i(0, \bar{\boldsymbol{q}}_L), \boldsymbol{v} = \boldsymbol{0}\}$
$\mathcal{X}(t_L, \bar{\boldsymbol{q}}_L)^\pm$	$\{\boldsymbol{x} : \boldsymbol{q} \in \mathcal{Q}(t_L, \bar{\boldsymbol{q}}_L)^\pm, \boldsymbol{v} = \boldsymbol{0}\}$
$e_{\boldsymbol{R}_L}$, e_{p_L}	load attitude and position errors

2) The impact of an internal force induced by nonvertical cables on the *robustness* of the load pose control is formally studied.
3) The effect of the internal force of diminishing the *sensitivity* of the load attitude error to parametric uncertainty or *variations* is shown.
4) A method for correcting the load position inaccuracy induced by the uncertainties is also presented.
5) We present extensive numerical results and hardware experiments supporting the claims conveyed by the theoretical analysis.
6) Last but not least, this article generalizes the system model by considering a generic position of the center of mass (CoM) of the load rather than assuming it to be in the middle of the cable anchoring points as done in [33].

The rest of this article is organized as follows. Section II contains some background useful to better understand the results of this article. In Sections III–V, we present the three main contributions of this article: Section III contains the derivation of the equilibrium points and Section IV their stability analysis; Section V highlights the role of the internal forces in the load error robustness and sensitivity to parametric variations. The results of the simulations and experiments are presented in Sections VI and VII, respectively. Finally, Section VIII concludes this article.

II. BACKGROUND

In this section, we provide the background needed to understand the contribution of this article. Specifically, we quickly recall the system's main variables, the dynamics equations, and the already established findings. For the sake of readability, the notation is also summarized in Tables I and II.

The considered system, sketched in Fig. 1, is the typical rigid beam load attached to two aerial robots through cables.

A. Load Model

The beam-like load has mass $m_L \in \mathbb{R}_{>0}$ and positive-definite rotational inertia $\boldsymbol{J}_L \in \mathbb{R}^{3\times3}$. The frame $\mathcal{F}_L =$

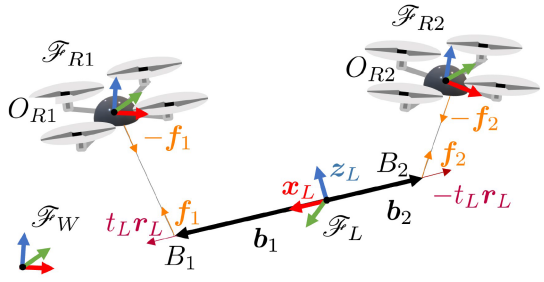

Fig. 1. Representation of the system and its major variables. The two aerial vehicles do not need to be necessarily quadrotors since the analysis and control design is valid for general aerial vehicles.

$\{O_L, \boldsymbol{x}_L, \boldsymbol{y}_L, \boldsymbol{z}_L\}$, where O_L coincides with the load CoM, is rigidly attached to the load. The inertial frame is denoted by $\mathscr{F}_W = \{O_W, \boldsymbol{x}_W, \boldsymbol{y}_W, \boldsymbol{z}_W\}$, where $\boldsymbol{z}_W$ is oriented in the direction opposite to the gravity. The position and orientation of $\mathscr{F}_L$ w.r.t. $\mathscr{F}_W$, defined by the vector[1] ${}^W\boldsymbol{p}_L \in \mathbb{R}^3$ and the rotation matrix $\boldsymbol{R}_L$, respectively, describe the full configuration of the load. We recall that the rotation along the axis that passes between the two cable anchoring points is not controllable by the robots. In the beam load, only the yaw angle ψ and the pitch angle θ are used to describe its attitude. The usual equations of a rigid body subject to gravity and contact forces describe the dynamics of the load as

$$\dot{\boldsymbol{v}}_L = \boldsymbol{M}_L^{-1}\left(-\boldsymbol{c}_L(\boldsymbol{v}_L) - \boldsymbol{g}_L + \boldsymbol{G}(\boldsymbol{q}_L)\boldsymbol{f}\right) \tag{1}$$

where $\boldsymbol{q}_L = (\boldsymbol{p}_L, \boldsymbol{R}_L)$; $\boldsymbol{v}_L = [\dot{\boldsymbol{p}}_L^\top \ {}^L\boldsymbol{\omega}_L{}^\top]^\top$ with ${}^L\boldsymbol{\omega}_L \in \mathbb{R}^3$ the angular velocity of $\mathscr{F}_L$ w.r.t. $\mathscr{F}_W$ expressed in $\mathscr{F}_L$; $\boldsymbol{M}_L = \mathrm{diag}(m_L\boldsymbol{I}_3, \boldsymbol{J}_L)$ with $\boldsymbol{I}_3 \in \mathbb{R}^{3\times3}$ the identity matrix; and $\boldsymbol{g}_L = [m_L g\boldsymbol{e}_3^\top \ \boldsymbol{0}]^\top$, where g is the gravitational acceleration and $\boldsymbol{e}_i$ is the canonical unit vector with a 1 in the ith entry. Coriolis and centrifugal terms are given by

$$\boldsymbol{c}_L = \begin{bmatrix} \boldsymbol{0} \\ \boldsymbol{S}(\boldsymbol{\omega}_L)\boldsymbol{J}_L\boldsymbol{\omega}_L \end{bmatrix}$$

where $\boldsymbol{S}(\star)$ is the *skew operator*,[2] and the grasp matrix is

$$\boldsymbol{G} = \begin{bmatrix} \boldsymbol{I}_3 & \boldsymbol{I}_3 \\ \boldsymbol{S}({}^L\boldsymbol{b}_1)\boldsymbol{R}_L^\top & \boldsymbol{S}({}^L\boldsymbol{b}_2)\boldsymbol{R}_L^\top \end{bmatrix}.$$

The load is suspended by two cables from two anchoring points, B_i with $i = 1, 2$, for which the position w.r.t. $\mathscr{F}_L$ is described by the vector ${}^L\boldsymbol{b}_i \in \mathbb{R}^3$. Each cable exerts on the load a force $\boldsymbol{f}_i$ such that $\boldsymbol{f} = [\boldsymbol{f}_1^\top \ \boldsymbol{f}_2^\top]^\top$ in (1). By simple kinematics, the position of B_i w.r.t. $\mathscr{F}_W$ is then given by $\boldsymbol{b}_i = \boldsymbol{p}_L + \boldsymbol{R}_L{}^L\boldsymbol{b}_i$. Since we are considering a beam-like load, the object CoM is aligned with the two anchoring points of the cables. Without loss of generality, we assume that ${}^L\boldsymbol{b}_1 = [b_1 \ 0 \ 0]^\top$ and ${}^L\boldsymbol{b}_2 = [-b_2 \ 0 \ 0]^\top$, where $b_i \in \mathbb{R}_{>0}$, for $i = 1, 2$. We also define the beam's length $L = b_1 + b_2$.

B. Robot Model

We define a frame $\mathscr{F}_{Ri} = \{O_{Ri}, \boldsymbol{x}_{Ri}, \boldsymbol{y}_{Ri}, \boldsymbol{z}_{Ri}\}$ rigidly attached to the ith robot and centered in its CoM. The ith cable is attached to the ith aerial vehicle at the point O_{Ri}, which allows decoupling the robot's attitude dynamics from the rest [25], [29]. $\mathscr{F}_{Ri}$ is used to describe the position and rotation of the vehicle w.r.t. $\mathscr{F}_W$, denoted by the vector $\boldsymbol{p}_{Ri} \in \mathbb{R}^3$ and the rotation matrix $\boldsymbol{R}_{Ri} \in SO(3)$, respectively.

The use of recent controllers for unidirectional- and multidirectional-thrust vehicles [39], [40] and disturbance observers for aerial vehicles has been experimentally proven to result in negligible tracking errors even in the presence of external disturbances.

Consequently, owing to the time-scale separation between the fast attitude dynamics and the slow translational dynamics [41], the closed-loop translational dynamics of the robot under the influence of the position controller effectively behaves like that of a double integrator $\ddot{\boldsymbol{p}}_{Ri} = \boldsymbol{u}_{Ri}$, where $\boldsymbol{u}_{Ri}$ is a virtual input. In other words, it is safe to assume that the aerial robots together with a sufficiently accurate position controller can track any desired C^2 trajectory with negligible error in the domain of interest [2], independently from external disturbances [33]. In this article, we follow such experimentally validated common practice for the theoretical derivations contained in Sections III–V (see, e.g., the experiments on cooperative load transport in [25] and [32]), and we utilize underactuated quadrotors for both the numerical and experimental validations in Sections VI and VII.

C. Cable Model

Cable-to-robot and cable-to-load connections are modeled as passive and mass-negligible rotational joints. Besides, the ith cable is represented as a unilateral spring along its principal direction, which is a frequently adopted model [33], [42], [43], [44]. As commonly done in the state of the art, the mass and inertia of cables are assumed negligible in comparison to those of the robots and loads. Its parameters are the constant elastic coefficient $k_i \in \mathbb{R}_{>0}$ and the constant rest length denoted by l_{0i}.

The attitude of the ith cable w.r.t. $\mathscr{F}_W$ is expressed by the normalized vector[3] $\boldsymbol{l}_i/\|\boldsymbol{l}_i\| \in \mathbb{S}^2$, where $\boldsymbol{l}_i = \boldsymbol{p}_{Ri} - \boldsymbol{b}_i$. The force acting on the load at B_i, given a certain length $\|\boldsymbol{l}_i\|$ of the cable, is given by simplified Hooke's law

$$\boldsymbol{f}_i = \|\boldsymbol{f}_i\|\frac{\boldsymbol{l}_i}{\|\boldsymbol{l}_i\|}, \quad \|\boldsymbol{f}_i\| = \begin{cases} k_i(\|\boldsymbol{l}_i\| - l_{0i}), & \text{if } \|\boldsymbol{l}_i\| - l_{0i} > 0 \\ 0, & \text{otherwise} \end{cases}. \tag{2}$$

The force produced, on the other hand, of the cable, i.e., on the ith robot at O_{Ri}, is equal to $-\boldsymbol{f}_i$.

D. Controller

We recall that to regulate the pose of the manipulated load to a desired configuration $\bar{\boldsymbol{q}}_L = (\bar{\boldsymbol{p}}_L, \bar{\boldsymbol{R}}_L)$, an admittance controller is used on the robots [33]:

$$\boldsymbol{u}_{Ri} = \boldsymbol{M}_{Ai}^{-1}\left(-\boldsymbol{B}_{Ai}\dot{\boldsymbol{p}}_{Ri} - \boldsymbol{K}_{Ai}\boldsymbol{p}_{Ri} - \boldsymbol{f}_i + \boldsymbol{\pi}_{Ai}\right) \tag{3}$$

where the positive-definite symmetric matrices $\boldsymbol{M}_{Ai}$, $\boldsymbol{B}_{Ai}, \boldsymbol{K}_{Ai} \in \mathbb{R}^{3\times3}$ are, respectively, the virtual inertia of the robot and the damping and stiffness coefficients of a virtual spring–damper system that links the robot and a desired reference frame; $\boldsymbol{\pi}_{Ai} \in \mathbb{R}^3$ is an additional forcing input that is properly set to steer the load to the desired configuration.

Remark 1: One can notice that (3) requires only local information, i.e., the robot's state $(\boldsymbol{p}_{Ri}, \dot{\boldsymbol{p}}_{Ri})$, which can be retrieved with standard onboard sensors, such as inertial measurement unit (IMU), global positioning system, and cameras, and the force applied by the cable $\boldsymbol{f}_i$ that can be directly measured by

[1] The left superscript indicates the reference frame. From now on, $\mathscr{F}_W$ is considered as a reference frame when the superscript is omitted.

[2] Given $\boldsymbol{x} \in \mathbb{R}^3$, $\boldsymbol{S}(\boldsymbol{x}) \in \mathbb{R}^{3\times3}$ is such that $\boldsymbol{S}(\boldsymbol{x})\boldsymbol{y} = \boldsymbol{x} \times \boldsymbol{y}$ for all $\boldsymbol{y} \in \mathbb{R}^3$.

[3] $\mathbb{S}^2 = \{\boldsymbol{v} \in \mathbb{R}^3 \mid \|\boldsymbol{v}\| = 1\}$

an onboard force sensor or estimated by a sufficiently precise model-based observer, as done in [25] and [45]. Therefore, the described method is decentralized and does not require explicit communication between the robots.

E. Closed-Loop Model

From (1) and (3), the closed-loop system dynamics can be written as $\dot{\boldsymbol{v}} = m(\boldsymbol{q}, \boldsymbol{v}, \boldsymbol{\pi}_A)$, where

$$m(\boldsymbol{q}, \boldsymbol{v}, \boldsymbol{\pi}_A) = \begin{bmatrix} \boldsymbol{M}_A^{-1}\left(-\boldsymbol{B}_A \boldsymbol{v}_R - \boldsymbol{K}_A \boldsymbol{q}_R - \boldsymbol{f} + \boldsymbol{\pi}_A\right) \\ \boldsymbol{M}_L^{-1}\left(-\boldsymbol{c}_L(\boldsymbol{v}_L) - \boldsymbol{g}_L + \boldsymbol{G}\boldsymbol{f}\right) \end{bmatrix} \tag{4}$$

with $\boldsymbol{q}_R = [\boldsymbol{p}_{R1}^\top \ \boldsymbol{p}_{R2}^\top]^\top$, $\boldsymbol{q} = (\boldsymbol{q}_R, \boldsymbol{q}_L)$, $\boldsymbol{v}_R = [\dot{\boldsymbol{p}}_{R1}^\top \ \dot{\boldsymbol{p}}_{R2}^\top]^\top$, $\boldsymbol{v} = [\boldsymbol{v}_R^\top \ \boldsymbol{v}_L^\top]^\top$, and $\boldsymbol{\pi}_A = [\boldsymbol{\pi}_{A1}^\top \ \boldsymbol{\pi}_{A2}^\top]^\top$. Furthermore, $\boldsymbol{M}_A = \mathrm{diag}(\boldsymbol{M}_{A1}, \boldsymbol{M}_{A2})$, $\boldsymbol{B}_A = \mathrm{diag}(\boldsymbol{B}_{A1}, \boldsymbol{B}_{A2})$, and $\boldsymbol{K}_A = \mathrm{diag}(\boldsymbol{K}_{A1}, \boldsymbol{K}_{A2})$. In order to coordinate the motion of the robots in a decentralized way, a *leader–follower* approach is used. In this way, only the designated leader will have active control over the position of the load. On the other hand, the other robot will follow, partially sustaining the weight of the load and contributing to the control of the load attitude. Choosing without loss of generality, robot 1 as the leader and robot 2 as the follower, the leader–follower approach is achieved as previously proposed in [25], [32], [33], and [34] by setting $\boldsymbol{K}_{A1} \neq \boldsymbol{0}$ and $\boldsymbol{K}_{A2} = \boldsymbol{0}$.

In the following, we present Theorem 1, from [33], along with two definitions that will help the reader comprehend the contribution of this article.

Definition 1 (Equilibrium configuration): $\boldsymbol{q}$ is an *equilibrium configuration*, indicated as $\bar{\boldsymbol{q}}$, if $\exists\, \boldsymbol{\pi}_A$ s.t. $\boldsymbol{0} = m(\boldsymbol{q}, \boldsymbol{0}, \boldsymbol{\pi}_A)$, i.e, if the corresponding zero-velocity state is a forced equilibrium for system (4) for a certain forcing input $\boldsymbol{\pi}_A$.

Definition 2 (Load internal force): For the considered system, the *load internal force* is defined as

$$t_L := \tfrac{1}{2}\boldsymbol{f}^\top \begin{bmatrix} \boldsymbol{I}_3 & -\boldsymbol{I}_3 \end{bmatrix}^\top \boldsymbol{R}_L \boldsymbol{e}_1 \tag{5}$$

where $\begin{bmatrix} \boldsymbol{I}_3 & -\boldsymbol{I}_3 \end{bmatrix}^\top \boldsymbol{R}_L \boldsymbol{e}_1 \in Ker(\boldsymbol{G})$. We have that:

1) if $t_L > 0$, the internal force causes a *tension* in the load;
2) if $t_L < 0$, the internal force causes a *compression*.

The following result, proven in [33], provides the expression of the forcing input $\boldsymbol{\pi}_A$ and the robot configurations $\boldsymbol{q}_R$, for which, given a desired load configuration $\bar{\boldsymbol{q}}_L$, $\boldsymbol{q} = (\boldsymbol{q}_R, \bar{\boldsymbol{q}}_L)$ is an equilibrium configuration of the system.

Theorem 1 (equilibrium inverse problem, provided in [33], reported here for completeness): Consider the closed-loop system (4) and assume that the load is at a given desired configuration $\bar{\boldsymbol{q}}_L = (\bar{\boldsymbol{p}}_L, \bar{\boldsymbol{R}}_L)$. For each internal force $t_L \in \mathbb{R}$, there exists a unique constant value of the forcing input $\boldsymbol{\pi}_A = \bar{\boldsymbol{\pi}}_A$ (and a unique position of the robots $\boldsymbol{q}_R = \bar{\boldsymbol{q}}_R$) such that $\bar{\boldsymbol{q}} = (\bar{\boldsymbol{q}}_L, \bar{\boldsymbol{q}}_R)$ is an equilibrium of the system.

In particular, $\bar{\boldsymbol{\pi}}_A$ and $\bar{\boldsymbol{q}}_R = [\bar{\boldsymbol{p}}_{R1}^\top \ \bar{\boldsymbol{p}}_{R2}^\top]^\top$ are given by

$$\bar{\boldsymbol{\pi}}_A(\bar{\boldsymbol{q}}_L, t_L) = \boldsymbol{K}_A \bar{\boldsymbol{q}}_R + \bar{\boldsymbol{f}}(\bar{\boldsymbol{q}}_L, t_L) \tag{6}$$

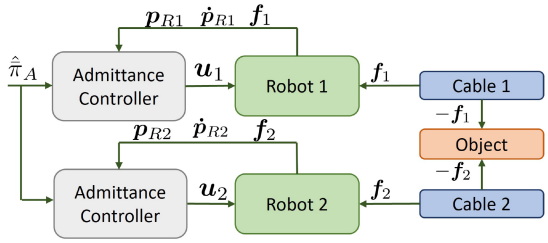

Fig. 2. Schematic representation of the overall system, including both the physical and control blocks. The input of the admittance controller is affected by the uncertainty of the system parameters.

$$\bar{\boldsymbol{p}}_{Ri}(\bar{\boldsymbol{q}}_L, t_L) = \bar{\boldsymbol{p}}_L + \bar{\boldsymbol{R}}_L {}^L\boldsymbol{b}_i + \left(\frac{\|\bar{\boldsymbol{f}}_i\|}{k_i} + l_{0i}\right)\frac{\bar{\boldsymbol{f}}_i}{\|\bar{\boldsymbol{f}}_i\|} \tag{7}$$

for $i = 1, 2$, where

$$\bar{\boldsymbol{f}}(\bar{\boldsymbol{q}}_L, t_L) = \begin{bmatrix} \bar{\boldsymbol{f}}_1 \\ \bar{\boldsymbol{f}}_2 \end{bmatrix} = \begin{bmatrix} \frac{b_2 m_L g}{\mathrm{L}} \\ \frac{b_1 m_L g}{\mathrm{L}} \end{bmatrix} \begin{bmatrix} \boldsymbol{I}_3 \\ \boldsymbol{I}_3 \end{bmatrix} \boldsymbol{e}_3 + t_L \begin{bmatrix} \boldsymbol{I}_3 \\ -\boldsymbol{I}_3 \end{bmatrix} \bar{\boldsymbol{R}}_L \boldsymbol{e}_1. \tag{8}$$

From (6), we can see that the forcing input is made up of two parts: one that depends on the robots' positions computed from the load equilibrium configuration according to kinematic relations, and the other that depends on the equilibrium forces. The equilibrium forces are composed, according to (8), of one term that compensates the gravity and one term that produces an internal force on the load whose intensity is t_L. Tognon et al. [33] confirm that, if $\bar{\boldsymbol{\pi}}_A$ is exactly applied to the closed-loop system (4), $\bar{\boldsymbol{q}}_L$ is an isolated load equilibrium configuration if $t_L \neq 0$, which is asymptotically stable if $t_L > 0$ and unstable if $t_L < 0$. Instead, $\bar{\boldsymbol{q}}_L$ belongs to a continuum of equilibrium points containing any possible attitude of the load if $t_L = 0$. In the remainder, Sections III–V contain the main theoretical contributions of this article.

III. Equilibria Under Uncertainty

In this section, the uncertainties are introduced, and the equilibrium configurations of the system subject to those uncertainties are derived.

Note that, in reality, $\bar{\boldsymbol{\pi}}_A$ in (6) cannot be applied exactly because of parametric uncertainties. Instead, one can apply only a version of $\bar{\boldsymbol{\pi}}_A$, denoted by $\hat{\bar{\boldsymbol{\pi}}}_A$, computed using the nominal uncertain values of the system parameters (see Fig. 2 for a schematic representation of the control scheme with the nominal forcing input). In the following, if not differently stated, we consider the general case in which a whole set of uncertainties is present. These uncertainties affect the control law (6) and, in turn, affect the system equilibrium configurations. The uncertainties are the following.

1) m_L is unknown, but only its nominal value $\hat{m}_L$ is available for the control design. We define the corresponding uncertainty as $\Delta_m = m_L - \hat{m}_L$.
2) b_1 is unknown, but only its nominal value $\hat{b}_1$ is available. The corresponding uncertainty, affecting the load CoM position, is $\Delta_b = b_1 - \hat{b}_1$.

3) L is unknown, but only its nominal value $\hat{L}$ is available, and we define $\Delta_\ell = \frac{1}{L} - \frac{1}{\hat{L}} = \ell - \hat{\ell}$ and $\Delta_L = L - \hat{L}$.
4) The model of the ith cable is inexact. Therefore, the nominal length l_{0i} and stiffness k_i are unknown, but their nominal values $\hat{l}_{0i}$ and $\hat{k}_i$ are available for the control design. We define the uncertainties $\Delta_{ki} = k_i - \hat{k}_i$ and $\Delta_{l_{0i}} = l_{0i} - \hat{l}_{0i}$.

Note that the nominal value of b_2 and $\hat{b}_2$ depends on the previously defined quantities according to $\hat{b}_2 = \hat{L} - \hat{b}_1$. However, for convenience, we also define $\Delta_{b2} = b_2 - \hat{b}_2$.

We shall now study the system's equilibrium configurations when $\hat{\bar{\boldsymbol{\pi}}}_A$ is applied.

Theorem 2 (Equilibrium direct problem): Given a desired load configuration $\bar{\boldsymbol{q}}_L = (\bar{\boldsymbol{p}}_L, \bar{\boldsymbol{R}}_L)$ and the internal force $t_L \in \mathbb{R}$, assume that the forcing input $\hat{\bar{\boldsymbol{\pi}}}_A$ is computed from (6) and is applied to the closed-loop system (4). Then, the equilibrium configurations are all and only the ones satisfying the following conditions:

$$\boldsymbol{p}_{R1} = \hat{\bar{\boldsymbol{p}}}_{R1} - \boldsymbol{K}_{A1}^{-1}(\Delta_m g \boldsymbol{e}_3) := \boldsymbol{p}_{R1}^{\text{eq}} \tag{9}$$

$$\boldsymbol{R}_L := \boldsymbol{R}_L^{\text{eq}} \text{ s.t. } \boldsymbol{S}(\boldsymbol{e}_1)\boldsymbol{R}_L^{\text{eq}\top}\left[\left(b_1 m_L - \frac{\hat{b}_1 \hat{m}_L L}{\hat{L}}\right) g\boldsymbol{e}_3 + L t_L \bar{\boldsymbol{R}}_L \boldsymbol{e}_1\right] = \boldsymbol{0} \tag{10}$$

$$\boldsymbol{f}_1 = m_L g \boldsymbol{e}_3 - \frac{\hat{m_L}\hat{b}_1 g}{\hat{L}}\boldsymbol{e}_3 + t_L \bar{\boldsymbol{R}}_L \boldsymbol{e}_1 := \boldsymbol{f}_1^{\text{eq}} \tag{11}$$

$$\boldsymbol{f}_2 = \frac{\hat{b_1}\hat{m}_L g}{\hat{L}}\boldsymbol{e}_3 - t_L \bar{\boldsymbol{R}}_L \boldsymbol{e}_1 = \hat{\bar{\boldsymbol{f}}}_2 := \boldsymbol{f}_2^{\text{eq}} \tag{12}$$

$$\boldsymbol{p}_L = \boldsymbol{p}_{R1}^{\text{eq}} - \boldsymbol{R}_L^{\text{eq}L}\boldsymbol{b}_1 - \left(\frac{\|\boldsymbol{f}_1^{\text{eq}}\|}{k_1} + l_{01}\right)\frac{\boldsymbol{f}_1^{\text{eq}}}{\|\boldsymbol{f}_1^{\text{eq}}\|} := \boldsymbol{p}_L^{\text{eq}} \tag{13}$$

where $\hat{\bar{\boldsymbol{p}}}_{R1}$ indicates the reference position of the leader robot computed as in (7), namely, starting from $\bar{\boldsymbol{p}}_L$ and $\bar{\boldsymbol{R}}_L$, but using the uncertain parameters.

Proof: $\hat{\bar{\boldsymbol{\pi}}}_A$ is defined according to (6), where (8) becomes

$$\hat{\bar{\boldsymbol{f}}}(\bar{\boldsymbol{q}}_L, t_L) = \begin{bmatrix}\hat{\bar{\boldsymbol{f}}}_1 \\ \hat{\bar{\boldsymbol{f}}}_2\end{bmatrix} = \begin{bmatrix}\frac{(\hat{L}-\hat{b}_1)\hat{m}_L g}{\hat{L}} \\ \frac{\hat{b}_1 \hat{m}_L g}{\hat{L}}\end{bmatrix}\begin{bmatrix}\boldsymbol{I}_3 \\ \boldsymbol{I}_3\end{bmatrix}\boldsymbol{e}_3 + t_L\begin{bmatrix}\boldsymbol{I}_3 \\ -\boldsymbol{I}_3\end{bmatrix}\bar{\boldsymbol{R}}_L\boldsymbol{e}_1. \tag{14}$$

The control (3) is

$$\boldsymbol{u}_{Ri} = \boldsymbol{M}_{Ai}^{-1}\left(-\boldsymbol{B}_{Ai}\dot{\boldsymbol{p}}_{Ri} - \boldsymbol{K}_{Ai}\boldsymbol{p}_{Ri}) - \boldsymbol{f}_i + \hat{\bar{\boldsymbol{\pi}}}_{Ai}\right).$$

Consider the equilibrium condition

$$\boldsymbol{0} = m(\boldsymbol{q}, 0, \hat{\bar{\boldsymbol{\pi}}}_A). \tag{15}$$

Equation (12) is obtained by substituting the last three lines of (14) into (15) and solving the equilibrium condition for the follower robot. Then, (12) can be substituted into the load translational equilibrium [lines 7, 8, and 9 of (15)] to retrieve (11). Equation (9) results from the first three lines of (15) using (11). Finally, (10) can be obtained using (11) and (12) in the last three equations of (15). Equation (13) is obtained applying the analogous of (42). □

Definition 3: Given a desired load configuration $\bar{\boldsymbol{q}}_L = (\bar{\boldsymbol{p}}_L, \bar{\boldsymbol{R}}_L)$, internal force $t_L \in \mathbb{R}$, and forcing input $\hat{\bar{\boldsymbol{\pi}}}_A = \hat{\bar{\boldsymbol{\pi}}}_A(\bar{\boldsymbol{q}}_L, t_L)$, we define the set of equilibrium configurations as $\mathscr{Q}(t_L, \bar{\boldsymbol{q}}_L) = \{\boldsymbol{q} \text{ s.t. conditions of Theorem 2 are satisfied}\}$

From Theorem 2, we can distinguish between two scenarios.

Scenario 1: If $t_L = 0$, condition (10) implies that the attitude of the load is such that $\boldsymbol{R}_L^{\text{eq}}\boldsymbol{e}_1$ is aligned to $\boldsymbol{e}_3$, and conditions (11) and (12) imply that both the cables are vertical. In other words, the load at the equilibrium is, irrespective of the parametric uncertainties, aligned with the vertical direction; even an infinitesimal parametric uncertainty would lead the load to this undesired configuration, in which the vertical load is aligned with the two vertical cables. Such a configuration is clearly not realizable. Note that the position error of the system at the equilibrium still depends on the parametric uncertainties [see condition (9)]. One can express the alignment between $\boldsymbol{R}_L^{\text{eq}}\boldsymbol{e}_1$ and $\boldsymbol{e}_3$ as $(\boldsymbol{R}_L^{\text{eq}}\boldsymbol{e}_1)^\top\boldsymbol{e}_3 = \pm 1$. By convention, let us indicate with $\mathscr{Q}_1(0, \bar{\boldsymbol{q}}_L)$ the system equilibrium configuration in which $(\boldsymbol{R}_L^{\text{eq}}\boldsymbol{e}_1)^\top\boldsymbol{e}_3 = +1$ holds, namely, the one in which the leader robot is above and the follower robot is below, and with $\mathscr{Q}_2(0, \bar{\boldsymbol{q}}_L)$ the other equilibrium configuration. Fig. 3(a) illustrates the aforementioned equilibrium configurations. Note also that there is an additional possibility. With simple manipulation, remembering that $\hat{b}_1 = b_1 + \Delta_b$, $\hat{b}_2 = b_2 + \Delta_{b2}$, and $\hat{L} = L + \Delta_L$ and defining ξ, the term in (10) becomes

$$\xi := \left(b_1 m_L - \frac{\hat{b}_1 \hat{m}_L L}{\hat{L}}\right) = \Delta_m b_1 + \frac{\Delta_{b2}}{\hat{L}}\hat{m}_L b_1 - \frac{\Delta_{b1}}{\hat{L}}\hat{m}_L b_2. \tag{16}$$

If $\xi = 0$, (10) is verified for every value of $\boldsymbol{R}_L$, and hence, the equilibrium configurations $\mathscr{Q}(0, \bar{\boldsymbol{q}}_L)$ are infinite such that the attitude of the load at equilibrium is arbitrary. This happens in the special case in which the parameters of the system are exactly known (this situation is the one we analyzed in [33] and which we can now see as a special case with $\xi = 0$). Indeed, $\xi = 0$ is also verified if the cable parameters are the sole uncertain ones, as it will also be more deeply discussed in the following. See Fig. 3(b) for a schematic representation of the mentioned equilibrium configurations.

Scenario 2: If $t_L \neq 0$, condition (10) holds when the vectors $\boldsymbol{R}_L^{\text{eq}}\boldsymbol{e}_1$ and

$$\left(\xi g \boldsymbol{e}_3 + L t_L \bar{\boldsymbol{R}}_L \boldsymbol{e}_1\right) \tag{17}$$

are aligned. Similar to before, this condition holds in two possible cases: when the vectors are aligned and point in the same direction, or when they are aligned but point in opposite directions. Let us indicate with $\boldsymbol{R}_L^{\text{eq}^+}$ the attitude of the load for which condition (10) holds and the two vectors $\boldsymbol{R}_L^{\text{eq}}\boldsymbol{e}_1$ and (17) point in the same direction. We indicate the corresponding load equilibrium configuration as $\mathscr{Q}^+(t_L, \bar{\boldsymbol{q}}_L)$. In the other case, when the two aforementioned vectors point in opposite directions, at the equilibrium, one has $\boldsymbol{R}_L^{\text{eq}^-} = \boldsymbol{R}_L^{\text{eq}^+}\boldsymbol{R}_{\boldsymbol{z}_L}(\pi)$; we indicate

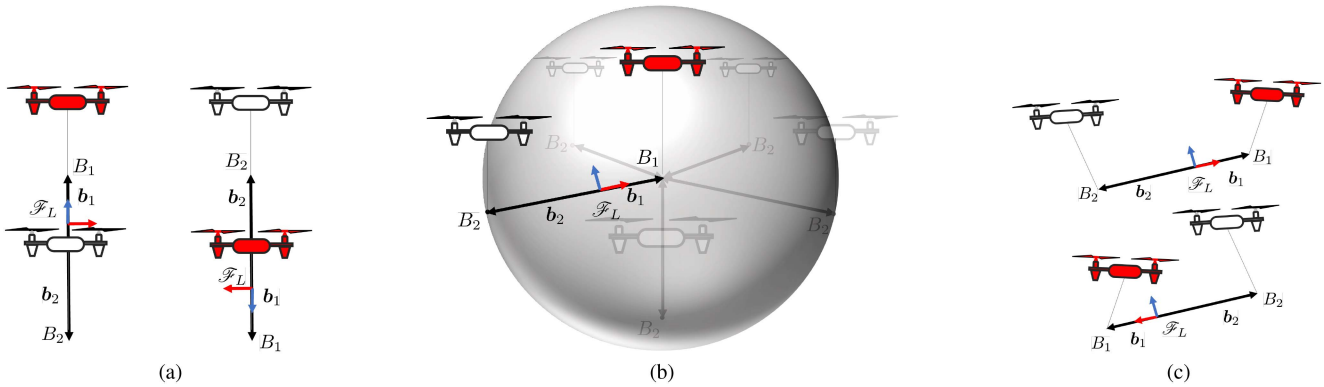

Fig. 3. Representation of different equilibrium configurations of the system depending on t_L and ξ. (a) $\mathcal{Q}(0, \bar{\boldsymbol{q}}_L)$ when $\xi \neq 0$. The position of the leader robot (in red) is the same in the two configurations. (b) $\mathcal{Q}(0, \bar{\boldsymbol{q}}_L)$ when $\xi = 0$. The position of the leader robot (in red) is the same in all the infinite equilibrium configurations, some of which are represented, and one of which is highlighted. Any other configuration with B_1 at the center of a sphere of radius L, B_2 on its surface, and the cables vertical is in $\mathcal{Q}(0, \bar{\boldsymbol{q}}_L)$ when $\xi = 0$. (c) $\mathcal{Q}(t_L, \bar{\boldsymbol{q}}_L)$ with $t_L \neq 0$. The position of the leader robot (in red) is the same in the two configurations. On top, the load is under tension; below, it is under compression.

the corresponding equilibrium configuration as $\mathcal{Q}^-(t_L, \bar{\boldsymbol{q}}_L)$. Depending on the sign of t_L in $\hat{\bar{\boldsymbol{\pi}}}_A$, the forces in the cables place the load under tension in one equilibrium configuration and under compression in the other. Fig. 3(c) represents these equilibrium configurations.

Remark 2: Under the hypothesis that $\bar{\theta} \neq \pi/2 + k\pi$, with $k \in \mathbb{N}$ and $t_L \neq 0$, as shown by (10), at the equilibrium, we have

$$\psi = \bar{\psi} + k\pi \tag{18}$$

$$\tan\theta = \tan\bar{\theta} + \frac{-\xi g}{L t_L \cos\bar{\theta}}. \tag{19}$$

In other words, *the uncertainties have no effect on the yaw angle at equilibrium.* ψ may differ from $\bar{\psi}$ by π because, as already discussed, both $\mathcal{Q}^+(t_L, \bar{\boldsymbol{q}}_L)$ and $\mathcal{Q}^-(t_L, \bar{\boldsymbol{q}}_L)$ are equilibrium configurations. Moreover, (19) tells us that not only is the attitude error proportional to the amount of uncertainty but also that, as t_L decreases, the load at the equilibrium becomes *increasingly vertical*. Eventually, for $t_L = 0$ and uncertain parameters ($\xi \neq 0$), (10) leads to $\boldsymbol{e}_1 \times \boldsymbol{R}_L^\top \boldsymbol{e}_3 = \boldsymbol{0}$. Namely, as previously observed, the load at the equilibrium is aligned with the vertical direction, and the two cables are vertical despite the value of $\xi \neq 0$. In other words, if $t_L = 0$, the load attitude error is unaffected by the parametric uncertainties: the load will reach the same, clearly undesired, configuration regardless of the smallest $\xi \neq 0$.

In the rest of this section, we briefly analyze the effects of each uncertain parameter on the final equilibrium.

A. Uncertainty on the Load Mass m_L

In this subsection, we only discuss uncertainty in the load's mass, while the other parameters are assumed to be perfectly known. Equations (9)–(12) become

$$\boldsymbol{p}_{R1}^{\text{eq}} = \hat{\bar{\boldsymbol{p}}}_{R1} - \boldsymbol{K}_{A1}^{-1} \Delta_m g \boldsymbol{e}_3 \tag{20}$$

$$b_1 \boldsymbol{S}(\boldsymbol{e}_1) \boldsymbol{R}_L^{\text{eq}\top} g \Delta_m \boldsymbol{e}_3 + t_L L \boldsymbol{S}(\boldsymbol{e}_1) \boldsymbol{R}_L^{\text{eq}\top} \bar{\boldsymbol{R}}_L \boldsymbol{e}_1 = \boldsymbol{0} \tag{21}$$

$$\boldsymbol{f}_1^{\text{eq}} = m_L g \boldsymbol{e}_3 - \frac{b_1 \hat{m}_L g}{L} \boldsymbol{e}_3 + t_L \bar{\boldsymbol{R}}_L \boldsymbol{e}_1 = \hat{\bar{\boldsymbol{f}}}_1 + \Delta_m g \boldsymbol{e}_3 \tag{22}$$

$$\boldsymbol{f}_2^{\text{eq}} = \frac{b_1 \hat{m}_L g}{L} \boldsymbol{e}_3 - t_L \bar{\boldsymbol{R}}_L \boldsymbol{e}_1 = \hat{\bar{\boldsymbol{f}}}_2. \tag{23}$$

The position of the load CoM at the equilibrium is different from $\bar{\boldsymbol{p}}_L$ and can be computed from (13) using (20)–(22).

It is worth noting that the leader robot can detect a mismatch between the known commanded $\hat{\bar{\boldsymbol{f}}}_1$ and the actual force $\boldsymbol{f}_1^{\text{eq}}$ measured at the steady state. Such a discrepancy solely depends on Δ_m, according to (22). Thus, the leader robot can compute Δ_m and, by knowing the nominal value $\hat{m}_L$, retrieve the actual value of the load mass m_L, which can be used to adjust its own reference force and position. However, note that in a communicationless setup, it is impossible for both the robots to know the correct parameter value based simply on their own state. In fact, according to (23), the follower robot has no mismatch between the equilibrium and the force reference value.

B. Uncertainty on the Load Length L or CoM Position b_1

Uncertainties on one of these two parameters have similar effects. In one case, $\hat{b}_1 \neq b_1$, namely, the load CoM is aligned to the cable attachment points on the load at an uncertain position but L is exactly known; in the other case, b_1 is exactly known but L is not. In both the cases, at the equilibrium, the following conditions hold:

$$\boldsymbol{p}_R^{\text{eq}} 1 = \hat{\bar{\boldsymbol{p}}}_{R1} \tag{24}$$

$$\boldsymbol{S}(\boldsymbol{e}_1) \boldsymbol{R}_L^{\text{eq}\top} (\text{Lt}_\text{L} \bar{\boldsymbol{R}}_L \boldsymbol{e}_1 + y m_L g \boldsymbol{e}_3) = \boldsymbol{0} \tag{25}$$

$$\boldsymbol{f}_1^{\text{eq}} = \hat{\bar{\boldsymbol{f}}}_1 \tag{26}$$

$$\boldsymbol{f}_2^{\text{eq}} = \hat{\bar{\boldsymbol{f}}}_2 \tag{27}$$

where $y = \Delta_b$ in one case, and $y = b_1 \text{L} \Delta_\ell$ in the other. $\hat{\bar{\boldsymbol{p}}}_{R1}$, $\hat{\bar{\boldsymbol{f}}}_1$, and $\hat{\bar{\boldsymbol{f}}}_2$ are computed from (7) and (8), where the corresponding uncertain parameter is used in place of the real one.

In this case, the leader robot position and both cable forces at the equilibrium coincide with the respective reference values available to the robots [see (24)–(27)]. Consequently, *it is not possible for any of the robots to estimate the uncertain parameter at the equilibrium based on the local information they possess.*

C. Uncertainty on the Cable Length l_{0i} or Stiffness k_i

Consider an uncertainty on the parameters of the ith cable such that the rest length is $l_{0i} \neq \hat{l}_{0i}$ and the stiffness is $k_i \neq \hat{k}_i$. At the equilibrium, $\boldsymbol{f}_i^{\text{eq}} = \bar{\boldsymbol{f}}_i$,

$$\boldsymbol{R}_L^{\text{eq}} = \bar{\boldsymbol{R}}_L \tag{28}$$

$$\boldsymbol{p}_{R1}^{\text{eq}} = \hat{\bar{\boldsymbol{p}}}_{R1} = \bar{\boldsymbol{p}}_L + \bar{\boldsymbol{R}}_L{}^L\boldsymbol{b}_1 + \left(\frac{\|\bar{\boldsymbol{f}}_1\|}{\hat{k}_1} + \hat{l}_{01}\right)\frac{\bar{\boldsymbol{f}}_1}{\|\bar{\boldsymbol{f}}_1\|} \tag{29}$$

and the value of $\boldsymbol{p}_L$ at the equilibrium is

$$\boldsymbol{p}_L^{\text{eq}} = \hat{\bar{\boldsymbol{p}}}_{R1} - \bar{\boldsymbol{R}}_L{}^L\boldsymbol{b}_1 - \left(\frac{\|\bar{\boldsymbol{f}}_1\|}{k_1} + l_{01}\right)\frac{\bar{\boldsymbol{f}}_1}{\|\bar{\boldsymbol{f}}_1\|}. \tag{30}$$

We highlight that knowledge about the cable properties is required only when computing the reference position of the leader robot, according to (7). What is more, only the information about k_1 and l_{01} is required. We conclude that the knowledge of l_{02} and k_2 is not necessary to stabilize the load at a desired pose. Moreover, l_{01} and k_1 have no effect on the load attitude at equilibrium, but they do influence the load position. This is evident by simply substituting (29) into (30) with $l_{01} \neq \hat{l}_{01}$ and $k_1 \neq \hat{k}_1$. Note that, since the robots' forces and the leader robot's position at the equilibrium coincide with the reference values available to the robots themselves, they are unaware of the load pose error induced by this uncertainty.

IV. Stability Analysis

In this section, we shall analyze the stability of the equilibrium configurations discovered in Section III. First, with $\boldsymbol{x} = (\boldsymbol{q}, \boldsymbol{v})$ being the state of the system, we define the following equilibrium states (subspaces of the state space).

1) $\mathscr{X}(0, \bar{\boldsymbol{q}}_L) = \{\boldsymbol{x} \ : \ \boldsymbol{q} \in \mathscr{Q}(0, \bar{\boldsymbol{q}}_L),\ \boldsymbol{v} = \boldsymbol{0}\}$.
2) $\mathscr{X}_1(0, \bar{\boldsymbol{q}}_L) = \{\boldsymbol{x} \ : \ \boldsymbol{q} \in \mathscr{Q}_1(0, \bar{\boldsymbol{q}}_L),\ \boldsymbol{v} = \boldsymbol{0}\}$.
3) $\mathscr{X}_2(0, \bar{\boldsymbol{q}}_L) = \{\boldsymbol{x} \ : \ \boldsymbol{q} \in \mathscr{Q}_2(0, \bar{\boldsymbol{q}}_L),\ \boldsymbol{v} = \boldsymbol{0}\}$.
4) $\mathscr{X}^+(t_L, \bar{\boldsymbol{q}}_L) = \{\boldsymbol{x} \ : \ \boldsymbol{q} \in \mathscr{Q}^+(t_L, \bar{\boldsymbol{q}}_L),\ \boldsymbol{v} = \boldsymbol{0}\}$.
5) $\mathscr{X}^-(t_L, \bar{\boldsymbol{q}}_L) = \{\boldsymbol{x} \ : \ \boldsymbol{q} \in \mathscr{Q}^-(t_L, \bar{\boldsymbol{q}}_L),\ \boldsymbol{v} = \boldsymbol{0}\}$.

Theorem 3: Let us consider a desired load configuration $\bar{\boldsymbol{q}}_L$. For the system (4), let the constant forcing input be $\hat{\bar{\boldsymbol{\pi}}}_A$. Then, we have the following.

1) $\mathscr{X}_1(0, \bar{\boldsymbol{q}}_L)$ is asymptotically stable if $\xi > 0$ and unstable if $\xi < 0$.
2) $\mathscr{X}_2(0, \bar{\boldsymbol{q}}_L)$ is asymptotically stable if $\xi < 0$ and unstable if $\xi > 0$.
3) $\mathscr{X}(0, \bar{\boldsymbol{q}}_L)$ is a set of marginally stable equilibrium points if $\xi = 0$.
4) $\mathscr{X}^+(t_L, \bar{\boldsymbol{q}}_L)$ is asymptotically stable.
5) $\mathscr{X}^-(t_L, \bar{\boldsymbol{q}}_L)$ is unstable.

Proof: Consider the following Lyapunov candidate function:

$$V(\boldsymbol{x}) = \frac{1}{2}(\boldsymbol{v}_R^\top \boldsymbol{M}_A \boldsymbol{v}_R + \boldsymbol{e}_R^\top \boldsymbol{K}_A \boldsymbol{e}_R + \boldsymbol{v}_L^\top \boldsymbol{M}_L \boldsymbol{v}_L + k_1(\|\boldsymbol{l}_1\| - l_{01})^2 + k_2(\|\boldsymbol{l}_2\| - l_{02})^2) - \boldsymbol{l}_1^\top \boldsymbol{f}_1^{\text{eq}} + - \boldsymbol{l}_2^\top \boldsymbol{f}_2^{\text{eq}} + V_0 + V_R(\boldsymbol{x}) \tag{31}$$

where the robot position error is $\boldsymbol{e}_R = \boldsymbol{p}_R - \boldsymbol{p}_R^{\text{eq}}$, V_0 is constant, and $V_R(\boldsymbol{x})$ is an additional term explained in the following. Function (31) is composed of standard positive-definite quadratic terms equal to zero in the equilibrium points, and by two terms of the form $\frac{1}{2}k_i(\|\boldsymbol{l}_i\| - l_{0i})^2) - \boldsymbol{l}_i{}^\top \boldsymbol{f}_i^{\text{eq}}$, call them $V_i(\boldsymbol{x})$: these are linked to the elastic energy of the cables and have a minimum at the equilibrium as well. A detailed proof of the former point can be found in [33]. The proof first shows that $V_i(\boldsymbol{x})$ is *radially unbounded*, i.e., $\lim_{\|\boldsymbol{x}\|\to\infty} V_i(\boldsymbol{x}) = \infty$. Then, based on this result and [46, Th. 1.15], the term has a global minimum. Finally, it has been shown that the global minimum of $V_i(\boldsymbol{x})$ corresponds to the considered equilibrium [33].

We define the value of $V_i(\boldsymbol{x})$ at the equilibrium (its minimum value) as $-V_0$, and we cancel it in (31) so that its value at the equilibrium is zero.

Let us start considering $\mathscr{X}_1(0, \bar{\boldsymbol{q}}_L)$ and $\xi > 0$. In this case, we set $V_R(\boldsymbol{x}) = \xi g(1 - \boldsymbol{e}_3^\top \boldsymbol{R}_L \boldsymbol{e}_1)$. With this choice, (31) is zero in $\mathscr{X}_1(0, \bar{\boldsymbol{q}}_L)$ because also the term $1 - \boldsymbol{e}_3^\top \boldsymbol{R}_L \boldsymbol{e}_1$ is zero in $\mathscr{X}_1(0, \bar{\boldsymbol{q}}_L)$ by definition (load aligned with the vertical with $\boldsymbol{R}_L \boldsymbol{e}_1$ and $\boldsymbol{e}_3$ pointing in the same direction) and positive elsewhere (the scalar product $\boldsymbol{e}_3^\top \boldsymbol{R}_L \boldsymbol{e}_1 \leq 1$ because $\boldsymbol{e}_3$ and $\boldsymbol{R}_L \boldsymbol{e}_1$ have both unit norm).

Studying the sign of the time derivative of (31), using (4), (2), and (8), we obtain $\dot{V}(\boldsymbol{x}) = -\boldsymbol{v}_R{}^\top \boldsymbol{B}_A \boldsymbol{v}_R$, which is clearly negative semidefinite. In particular, let us define $\mathscr{E} = \{\boldsymbol{x} \ : \ \dot{V}(\boldsymbol{x}) = 0\}$. In this case, we have $\mathscr{E} = \{\boldsymbol{x} \ : \ \boldsymbol{v}_R = \boldsymbol{0},\ \boldsymbol{\omega}_L = \boldsymbol{0}\}$.

Since $\dot{V}(\boldsymbol{x})$ is only negative *semi*definite, we rely on *LaSalle's invariance principle* to complete the proof: one can easily verify from (4) that the largest invariant set in $\mathscr{E}$ is $\mathscr{X}_1(0, \bar{\boldsymbol{q}}_L)$.

Analogous reasoning can be used when $\xi < 0$. The computation of $\dot{V}$ does not change, and it is, thus, negative semidefinite. However, $\mathscr{X}_1(0, \bar{\boldsymbol{q}}_L)$ is a set of accumulation for the points, where $V(\boldsymbol{x}) < 0$ if $\xi < 0$. To see this, consider $\boldsymbol{v} = \boldsymbol{0}$ and all quantities at the equilibrium apart from $\boldsymbol{R}_L$, which is such that $\boldsymbol{e}_3^\top \boldsymbol{R}_L \boldsymbol{e}_1 = 1 - \epsilon$, with $\epsilon > 0$ arbitrarily small, meaning that $\boldsymbol{R}_L$ is arbitrarily close to $\boldsymbol{R}_L^{\text{eq}}$. Under these conditions, $V(\boldsymbol{x}) = g\xi\epsilon < 0$. All the conditions of *Chetaev's theorem* (the formulation of both this and LaSalle's invariance principle can be found, e.g., in [47]) are satisfied. Hence, we can conclude that $\mathscr{X}^+(t_L, \bar{\boldsymbol{q}}_L)$ is unstable. To show that $\mathscr{X}_2(0, \bar{\boldsymbol{q}}_L)$ is asymptotically stable if $\xi < 0$, we set $V_R(\boldsymbol{x}) = -\xi g(1 + \boldsymbol{e}_3^\top \boldsymbol{R}_L \boldsymbol{e}_1)$, which is zero in $\mathscr{X}_2(0, \bar{\boldsymbol{q}}_L)$ (when $\boldsymbol{e}_3^\top \boldsymbol{R}_L \boldsymbol{e}_1 = -1$ by definition), and positive elsewhere. The same Lyapunov candidate function is used to show that $\mathscr{X}_2(0, \bar{\boldsymbol{q}}_L)$ is unstable if $\xi > 0$. The reasoning is exactly dual to the previous case; hence, it is here omitted for the sake of space.

Consider now $\xi = 0$. We set $V_R(\boldsymbol{x}) = 0$, so that (31) is zero in $\mathscr{X}(0, \bar{\boldsymbol{q}}_L)$ and positive elsewhere. Moreover, $\dot{V}$ is negative semidefinite as before. One can easily show that the largest invariant set is $\mathscr{X}(0, \bar{\boldsymbol{q}}_L)$. We can, thus, say that the system state converges to a state $\boldsymbol{x} \in \mathscr{X}(0, \bar{\boldsymbol{q}}_L)$, which is, however, composed of a continuum of equilibrium points. Hence, they are only *marginally* stable.

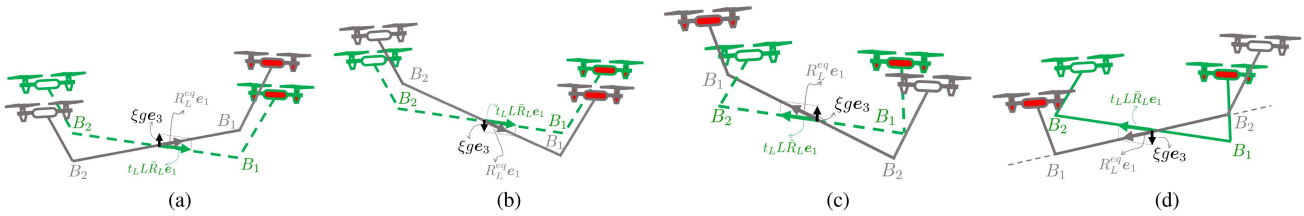

Fig. 4. Load attitude in the asymptotically stable equilibrium points $\mathscr{X}^+(t_L, \bar{\boldsymbol{q}}_L)$ when $t_L \neq 0$. The desired configuration is in dashed green, and the system with the actual attitude at the equilibrium is in gray. The leader robot is red. In $\mathscr{X}^+(t_L, \bar{\boldsymbol{q}}_L)$, the attitude at the equilibrium is always such that $\boldsymbol{R}_L^{\text{eq}}\boldsymbol{e}_1$ is aligned with $t_L\bar{\boldsymbol{R}}_L\boldsymbol{e}_1$. However, for $t_L < 0$, this means that the system is "flipped" compared to the desired configuration. (a) $t_L > 0$, $\xi > 0$. (b) $t_L > 0$, $\xi < 0$. (c) $t_L < 0$, $\xi > 0$. (d) $t_L < 0$, $\xi < 0$.

Finally, we study the stability of the equilibrium points when $t_L \neq 0$. In this case, we set $V_R(\boldsymbol{x}) = -(\xi g\boldsymbol{e}_3 + t_L L\bar{\boldsymbol{R}}_L\boldsymbol{e}_1)^\top \boldsymbol{R}_L\boldsymbol{e}_1 + V_0'$, with $V_0' = (\xi g\boldsymbol{e}_3 + t_L L\bar{\boldsymbol{R}}_L\boldsymbol{e}_1)^\top \boldsymbol{R}_L^{\text{eq}}\boldsymbol{e}_1$. Clearly, $V_R(\boldsymbol{x})$ and hence $V(\boldsymbol{x})$ are zero at the equilibrium. Moreover, $V_R(\boldsymbol{x})$ is positive elsewhere by definition of $\mathscr{X}^+(t_L, \bar{\boldsymbol{q}}_L)$ ($\xi g\boldsymbol{e}_3 + t_L L\bar{\boldsymbol{R}}_L\boldsymbol{e}_1$ and $\boldsymbol{R}_L\boldsymbol{e}_1$ are aligned and point in the same direction when $\boldsymbol{R}_L = \boldsymbol{R}_L^{\text{eq}}$, so that $V_R(\boldsymbol{x})$ has its minimum in $\mathscr{X}^+(t_L, \bar{\boldsymbol{q}}_L)$). Moreover, $\dot{V}(\boldsymbol{x}) = -\boldsymbol{v}_R{}^\top \boldsymbol{B}_A \boldsymbol{v}_R$, and the application of LaSalle's invariance principle leads to the conclusion that $\mathscr{X}^+(t_L, \bar{\boldsymbol{q}}_L)$ is an asymptotically stable equilibrium point, similarly to before. To show the instability of $\mathscr{X}^-(t_L, \bar{\boldsymbol{q}}_L)$, we use the same choice for $V_R(\boldsymbol{x})$. However, since $\xi g\boldsymbol{e}_3 + t_L L\bar{\boldsymbol{R}}_L\boldsymbol{e}_1$ and $\boldsymbol{R}_L\boldsymbol{e}_1$ are antiparallel in $\mathscr{X}^-(t_L, \bar{\boldsymbol{q}}_L)$, $V_R(\boldsymbol{x})$ is still zero at the equilibrium but negative when $\boldsymbol{R}_L$ is arbitrarily close to $\boldsymbol{R}_L^{\text{eq}}$. $\mathscr{X}^-(t_L, \bar{\boldsymbol{q}}_L)$ is a point of accumulation for the points in which $\dot{V}(\boldsymbol{x})$ is negative, while $\dot{V}(\boldsymbol{x})$ remains negative semidefinite. For Chetaev's theorem, we conclude that $\mathscr{X}^-(t_L, \bar{\boldsymbol{q}}_L)$ is unstable. □

It is important to highlight that, as shown in Fig. 4, for $t_L > 0$, $\mathscr{X}^+(t_L, \bar{\boldsymbol{q}}_L)$ corresponds to a configuration of the system in which $\boldsymbol{R}_L^{\text{eq}}$ (irrespective of the sign of ξ) is the closest condition to $\bar{\boldsymbol{R}}_L$, namely to the desired attitude, with a displacement due to the parametric uncertainty. Instead, for $t_L < 0$, $\mathscr{X}^-(t_L, \bar{\boldsymbol{q}}_L)$ is the equilibrium point in which the configuration of the load is the closest to the desired one. We can say that these configurations are the most desirable equilibrium configurations of the load in the presence of parametric uncertainties. As stated in Theorem 3, $t_L > 0$ stabilizes the most desirable equilibrium configuration of the load, which is, instead, unstable if $t_L < 0$.

V. Role of the Internal Forces on the Load Error Caused by Parametric Uncertainties

In this section, we provide a formal analysis of the role that the internal force plays in determining the load pose at the equilibrium in the presence of parametric uncertainties. We shall consider the simultaneous presence of all the uncertainties listed in Section III. We start considering the load *attitude*.

A. Load Attitude Error

Theorem 4: The load attitude error at the equilibrium $e_{\boldsymbol{R}_L}$, is inversely proportional to the intensity of a positive internal force t_L. Furthermore, defining

$$e_{\boldsymbol{R}_L} = \|\boldsymbol{R}_L\boldsymbol{e}_1 \times \bar{\boldsymbol{R}}_L\boldsymbol{e}_1\|^2 \tag{32}$$

the error sensitivity w.r.t. Δ_m, Δ_b, Δ_{k_i}, $\Delta_{l_{0i}}$, and Δ_ℓ, defined as $\frac{\partial e_{\boldsymbol{R}_L}}{\partial \Delta_m}$, $\frac{\partial e_{\boldsymbol{R}_L}}{\partial \Delta_b}$, $\frac{\partial e_{\boldsymbol{R}_L}}{\partial \Delta_{k_i}}$, $\frac{\partial e_{\boldsymbol{R}_L}}{\partial \Delta_{l_{0i}}}$, and $\frac{\partial e_{\boldsymbol{R}_L}}{\partial \Delta_\ell}$, respectively, is given by

$$\frac{\partial e_{\boldsymbol{R}_L}}{\partial \Delta_m} = \frac{-2\hat{b}_1\hat{\ell}g^2\alpha\cos\theta^2}{t_L^2L^2} \tag{33}$$

$$\frac{\partial e_{\boldsymbol{R}_L}}{\partial \Delta_b} = \frac{-2\hat{m}_L\hat{\ell}g^2\alpha\cos\theta^2}{t_L^2L^2} \tag{34}$$

$$\frac{\partial e_{\boldsymbol{R}_L}}{\partial \Delta_{ki}} = \frac{\partial e_{\boldsymbol{R}_L}}{\partial \Delta_{l0i}} = 0 \tag{35}$$

$$\frac{\partial e_{\boldsymbol{R}_L}}{\partial \Delta_\ell} = \frac{-2\hat{b}_1\hat{m}_Lg^2\alpha\cos\theta^2}{t_L^2L^2} \tag{36}$$

where $\alpha := (b_1 - \Delta b)(m_L - \Delta m)(\ell - \Delta_\ell) - m_L b_1$.

Proof: With a positive internal force, at the equilibrium, (18) with $k = 0$ holds. Thus, the quantity $|\theta^{eq} - \bar{\theta}|$ is a viable indicator of the attitude error. According to (19) and for monotonicity of the tan() function, the difference between $\bar{\theta}$ and θ^{eq} varies with the quantity $\xi g/(Lt_L\cos\bar{\theta})$, which is inversely proportional to t_L. Hence, the error is also inversely proportional to t_L. Now, rewrite (10) in $\mathscr{F}_W$ as

$$\boldsymbol{R}_L^{\text{eq}}\boldsymbol{e}_1 \times \left[\left(b_1m_L - \frac{\hat{b}_1\hat{m}_LL}{\hat{L}}\right)g\boldsymbol{e}_3 + Lt_L\bar{\boldsymbol{R}}_L\boldsymbol{e}_1\right] = \boldsymbol{0}. \tag{37}$$

Define also

$$\frac{\hat{b}_1\hat{m}_LL - b_1m_L\hat{L}}{t_LL\hat{L}}(\boldsymbol{R}_L^{\text{eq}}\boldsymbol{e}_1 \times g\boldsymbol{e}_3) := \boldsymbol{x}. \tag{38}$$

Thus, from (37), we have that $\boldsymbol{R}_L^{\text{eq}}\boldsymbol{e}_1 \times \bar{\boldsymbol{R}}_L\boldsymbol{e}_1 = \boldsymbol{x}$ and, from (32), that $e_{\boldsymbol{R}_L} = \boldsymbol{x}^\top\boldsymbol{x}$. Regarding the sensitivity, we show the proof for (33) only, because the other cases follow the exactly same analysis. We can write the sensitivity as

$$\frac{\partial e_{\boldsymbol{R}_L}}{\partial \Delta_m} = 2\boldsymbol{x}^\top\frac{\partial \boldsymbol{x}}{\partial \Delta_m} =$$

$$= 2\left[\frac{1}{t_LL}\boldsymbol{R}_L\boldsymbol{e}_1 \times (\alpha)g\boldsymbol{e}_3\right]^\top\left[\frac{1}{t_LL}\boldsymbol{R}_L\boldsymbol{e}_1 \times (\Delta b - b_1)g\boldsymbol{e}_3\right]. \tag{39}$$

Eventually, (39) can be rewritten as (33) by remembering that, given three vectors $\boldsymbol{a}, \boldsymbol{b}$, and $\boldsymbol{c}$

$$(\boldsymbol{a} \times \boldsymbol{b})^\top (\boldsymbol{a} \times \boldsymbol{c}) = |\boldsymbol{a}|^2 (\boldsymbol{b}^\top \boldsymbol{c}) - (\boldsymbol{a}^\top \boldsymbol{b})(\boldsymbol{a}^\top \boldsymbol{c}).$$

Note that we are considering $t_L \neq 0$ by assumption. □

Remark 3: The definition in (32) is a suitable metric for the attitude error if we consider the equilibrium point $\mathscr{X}^+(t_L, \bar{\boldsymbol{q}}_L)$, namely, the one in which the displacement between $\boldsymbol{R}_L^{\text{eq}} \boldsymbol{e}_1$ and $\bar{\boldsymbol{R}}_L \boldsymbol{e}_1$ is the smallest and, hence, our desired equilibrium point. First, $\boldsymbol{R}_L \boldsymbol{e}_1$ is enough to describe the entire attitude of the *beam-like* load. Second, $e_{\boldsymbol{R}_L}$ is zero when $\boldsymbol{R}_L^{\text{eq}} = \bar{\boldsymbol{R}}_L$ and increases with the displacement between the two vectors $\boldsymbol{R}_L^{\text{eq}} \boldsymbol{e}_1$ and $\bar{\boldsymbol{R}}_L \boldsymbol{e}_1$, at least locally (for displacements smaller than $\pm\pi/2$).

Moreover, Theorem 4 shows that increasing the intensity of the internal force t_L not only makes the attitude error smaller in the presence of parametric uncertainties, but also makes the error more *robust to variations of such uncertainties.*

This last aspect may be of particular practical interest: as a matter of fact, parametric uncertainty variations take place every time the actual physical parameters of the system change. A possible real-world scenario is the transportation of objects that are slightly different from each other, e.g., in mass and length. One may want to transport the objects without changing every time the controller parameters for the sake of time, thus dealing with varying parametric uncertainties. Especially interesting, as also highlighted in [48], is the variation affecting the CoM position, which may change online when transporting moving masses, i.e., containers of liquids, or boxes with smaller objects free to move inside. The previous analysis suggests that in all these cases, having a larger value of t_L is of uttermost benefit, resulting in an error less sensitive to the aforementioned parametric variations.

B. Load Position Error

Differently from what happens to the load attitude error, the load position error at the equilibrium does not necessarily decrease when t_L increases. While to claim a positive statement a comprehensive proof is needed, as we did in Section V-A, to deny a positive statement, as we do in this section, a counterexample is enough. First, it is easy to see that, when only l_{01} is uncertain, the load position error at the equilibrium, $\boldsymbol{e}_{p_L} := \boldsymbol{p}_L^{\text{eq}} - \bar{\boldsymbol{p}}_L$, is

$$\boldsymbol{e}_{p_L} = \Delta_l \frac{b_2 m g \boldsymbol{e}_3 + t_L \bar{\boldsymbol{R}}_L \boldsymbol{e}_1}{\| b_2 m g \boldsymbol{e}_3 + t_L \bar{\boldsymbol{R}}_L \boldsymbol{e}_1 \|}. \tag{40}$$

Equation (40) suggests that $\boldsymbol{e}_{p_L}$ is equal to a unit vector multiplied by $\Delta_{l_{01}}$; thus, its module is independent of the value of t_L. Moreover, in the next section, we provide two numerical examples showing that, depending on the specific combination and values of uncertainties, $\boldsymbol{e}_{p_L}$ may even have a nonmonotonic evolution for increasing values of t_L, with an initial increase or decay.

We show, however, that the load position error at the equilibrium can be corrected, ideally to zero, without altering the leader–follower architecture or requiring direct communication between the robots.

We recall that, due to parametric uncertainties, the reference position given to the leader robot is

$$\hat{\bar{\boldsymbol{p}}}_{R1} = \bar{\boldsymbol{p}}_L + \bar{\boldsymbol{R}}_L {}^L\hat{\boldsymbol{b}}_1 + \left(\frac{\| \hat{\bar{\boldsymbol{f}}}_1 \|}{\hat{k}_1} + \hat{l}_{01} \right) \frac{\hat{\bar{\boldsymbol{f}}}_1}{\| \hat{\bar{\boldsymbol{f}}}_1 \|}. \tag{41}$$

By using kinematics, (9), and (41), the load position at the equilibrium is

$$\begin{aligned} \boldsymbol{p}_L^{\text{eq}} &= \boldsymbol{p}_{R1}^{\text{eq}} - \left(\frac{\| \boldsymbol{f}_1^{\text{eq}} \|}{k_1} + l_{01} \right) \frac{\boldsymbol{f}_1^{\text{eq}}}{\| \boldsymbol{f}_1^{\text{eq}} \|} - \boldsymbol{R}_L^{\text{eq}} \boldsymbol{b}_1 \\ &= \bar{\boldsymbol{p}}_L + \bar{\boldsymbol{R}}_L {}^L\hat{\boldsymbol{b}}_1 + \left(\frac{\| \hat{\bar{\boldsymbol{f}}}_1 \|}{\hat{k}_1} + \hat{l}_{01} \right) \frac{\hat{\bar{\boldsymbol{f}}}_1}{\| \hat{\bar{\boldsymbol{f}}}_1 \|} - K_A^{-1} \Delta_m g \boldsymbol{e}_3 + \\ &- \left(\frac{\| \boldsymbol{f}_1^{\text{eq}} \|}{k_1} + l_{01} \right) \frac{\boldsymbol{f}_1^{\text{eq}}}{\| \boldsymbol{f}_1^{\text{eq}} \|} - \boldsymbol{R}_L^{\text{eq}} \boldsymbol{b}_1. \end{aligned} \tag{42}$$

From (42), we have an expression for $\boldsymbol{e}_{p_L}$. Now, *if the leader robot knows the load position*, it can recognize that, at steady state, $\tilde{\boldsymbol{p}_L} \neq 0$ holds, and it can adjust its position reference to ${}^2\hat{\bar{\boldsymbol{p}}}_{R1}$ accordingly, with

$${}^2\hat{\bar{\boldsymbol{p}}}_{R1} = \hat{\bar{\boldsymbol{p}}}_{R1} - \boldsymbol{e}_{p_L}. \tag{43}$$

In this way, there will be a new equilibrium, in which the leader robot position is

$$\boldsymbol{p}_{R1}^{\text{eq}} = {}^2\hat{\bar{\boldsymbol{p}}}_{R1} - K_A^{-1} \Delta_m g \boldsymbol{e}_3 \tag{44}$$

and, thus, (42) becomes

$$\boldsymbol{p}_L^{\text{eq}} = \bar{\boldsymbol{p}}_L. \tag{45}$$

It is important to highlight that the leader robot position only influences the load position and not the attitude at the equilibrium, which depends only upon the reference forces computed based on $\bar{\boldsymbol{R}}_L$. Indeed, by evaluating (4) at the equilibrium, the last three rows are

$$\boldsymbol{S}({}^L\boldsymbol{b}_1) \boldsymbol{R}_L^{\text{eq}\top} \boldsymbol{f}_1^{\text{eq}} + \boldsymbol{S}({}^L\boldsymbol{b}_2) \boldsymbol{R}_L^{\text{eq}\top} \boldsymbol{f}_2^{\text{eq}} = \boldsymbol{0}$$

which becomes, substituting $\boldsymbol{f}_i^{\text{eq}}$, (10). Hence, the leader robot can correct the load position error, while the internal force independently acts decreasing the attitude error. Because the load's position can be steered relying solely on the leader robot, unlike the load's attitude, which is determined by the cooperative actions of both robots, the control approach can maintain its distributed nature. However, to correct the load position error, the leader robot must have access to the load position. This implies that the leader robot would require additional sensors, such as cameras to accomplish this task.

VI. Numerical Validation

Extensive numerical simulations have been carried out using a URDF description of the system and ODE physics engine in Gazebo. We avoided validating the theoretical results on the same equations used to derive them. The main differences between the control model used to derive a fully satisfactory theoretical analysis and the complex simulation model used to study the applicability of the theoretical results in the real world are as follows.

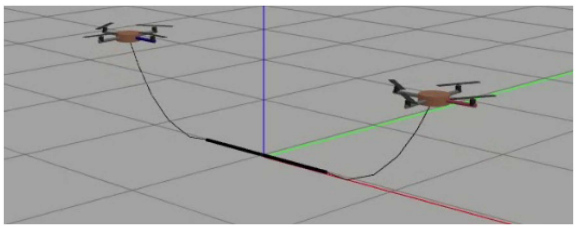

Fig. 5. Sagging cable model in the simulated scenario.

1) Underactuated quadrotors have been preferred for the validation since they represent the worst case in terms of the validity of some of the assumptions made in the theoretical analyses. Validation using fully actuated aerial robots would have seemed, instead, limiting.
2) The cables are subject to sagging, which is obtained by using a series of several links interconnected by passive universal joints, as can be seen in Fig. 5.
3) In the validation, there is no guarantee of perfect trajectory tracking as assumed in the theory, but a standard position controller [49] is implemented for each robot.
4) The wrench observer proposed in [50] is used to estimate the force applied by the cable on the robot. The observer introduces noisy and delayed measurements when compared to ideal force measurement.

The control software has been implemented in MATLAB-Simulink using the Generator of Modules GenoM.[4] The interface between MATLAB and Gazebo is also managed by a Gazebo-genom3 plugin.[5] All the phases of a physical experiment, starting with takeoff, are replicated in the simulated environment using a state machine, ensuring that the results are as realistic as possible. After the takeoff, the two robots lift the load, and the admittance controller is activated right after.

The robot models are two quadrotors weighing 1.03 kg and having a maximum thrust for each propeller of 6 N. They are equipped with two light cables of length 1 m and attached to a bar. The bar is a 1-m-long link with a mass of 0.5 kg.

A. Case of $t_L > 0$

Fig. 6 contains the average load attitude error at a steady state in a total of 40 simulations. The average is computed in a 2s time window. In all those simulations, $\bar{\boldsymbol{p}}_L = [1\ 1\ 1]^\top$ m, the load desired yaw is $\bar{\psi} = \frac{\pi}{8}$ rad, and the desired pitch $\bar{\theta} = -\frac{\pi}{12}$ rad. In each of the three plots in Fig. 6, for four different values of the internal force, $t_L = \{0.5,\ 0.75,\ 1,\ 1.25\}$N, four different simulation results are displayed for each relative error equal to 0%, 5%, 10%, and 15% on a specific uncertain parameter considered separately from the others. Specifically, Fig. 6(a) considers the uncertainty on m_L, Fig. 6(b) on L, and Fig. 6(c) on b_1. Even in the absence of uncertainties, small errors of less than 2.5° in the bar's attitude control can be found. This can be due to minor tracking errors or possible biases in the wrench observer, which estimations are unbiased as soon as the robot takes off. These considerations ignore the external forces applied by the loose cables at the startup phase. From all the three figures, one can appreciate the beneficial effect of larger values of t_L on the attitude error: for the same value of the uncertainty, the attitude error decreases if t_L increases. Moreover, the plots show that for every value of t_L, increasing the uncertainty on one parameter increases the attitude error, as expected, but, especially, the increase is smaller for high values of t_L (this can be seen by the slope of the lines in the plots). These results confirm the theoretical findings collected in Theorem 4. Fig. 7(a) and (b) provides validation of the theoretical results on the effect of the uncertainties affecting the cable parameters. The leader robot position reference is not given as a step, but the robot follows a fifth-order polynomial trajectory to reach the desired position. An error of 15% is considered to affect the length of the leader and follower robot's cable in Fig. 7(a) and (b), respectively. In both the cases, $t_L = 1$N. Note that the displayed time starts after the admittance controller activation. The reader can appreciate how uncertainties on the leader robot's cable model only cause $\boldsymbol{p}_L^{\text{eq}} \neq \bar{\boldsymbol{p}}_L$, while $\boldsymbol{R}_L^{\text{eq}} = \bar{\boldsymbol{R}}_L$, and how the follower robot's cable parameters are not needed to control the load pose, as expected from (28) and (30).

[4][Online]. Available: https://git.openrobots.org/projects/genom3
[5][Online]. Available: https://git.openrobots.org/projects/mrsim-gazebo

B. Case of $t_L < 0$

Fig. 7(a) and (b) provides validation of the theoretical results on the effect of the uncertainties affecting the cable parameters. The leader robot position reference is not given as a step, but the robot follows a fifth-order polynomial trajectory to reach the desired position. An error of 15% is considered to affect the length of the leader and follower robot's cable in Fig. 7(a) and (b), respectively. In both the cases, $t_L = 1$N. Note that the displayed time starts after the admittance controller activation. The reader can appreciate how uncertainties on the leader robot's cable model only cause $\boldsymbol{p}_L^{\text{eq}} \neq \bar{\boldsymbol{p}}_L$, while $\boldsymbol{R}_L^{\text{eq}} = \bar{\boldsymbol{R}}_L$, and how the follower robot's cable parameters are not needed to control the load pose, as expected from (28) and (30).

C. Case of $t_L < 0$

Here, we show the behavior of the system with $t_L < 0$. The unstable nature of the desired configuration with no parametric uncertainties was shown in [33]. The simulations of the realistic system, in accordance with Theorem 3, show that $\mathscr{X}^-(t_L, \bar{\boldsymbol{q}}_L)$ is unstable when the parametric uncertainties are considered. We report the results of two simulations with $\bar{\boldsymbol{p}}_{R1} = [0\ 0\ 1]^\top$ m, $\bar{\psi} = \frac{\pi}{8}$ rad, and $\bar{\theta} = 0$ rad (desired horizontal bar). We simulate an uncertainty of 5% both on m_L and L such that: 1) $\xi > 0$ (we chose $\hat{m}_L < m_L$ and $\hat{L} > L$) and 2) $\xi < 0$ (thanks to $\hat{m}_L > m_L$ and $\hat{L} < L$). In both the cases, we obtained that, in accordance to Theorem 3, the system converges to $\mathscr{X}^+(t_L, \bar{\boldsymbol{q}}_L)$. Since $t_L < 0$, this means, as reported in Fig. 8, that we have $\psi^{\text{eq}} = \bar{\psi} - \pi$, while θ^{eq} varies according to the sign of ξ, as expected (see Fig. 4). The cable forces were observed to be as desired, except for the vertical component of $\bar{\boldsymbol{f}}_1$, as expected due to $\Delta_m \neq 0$ according to (22). Fig. 8 shows the behavior of the system in the described cases through screenshots of the Gazebo environment, and Fig. 9

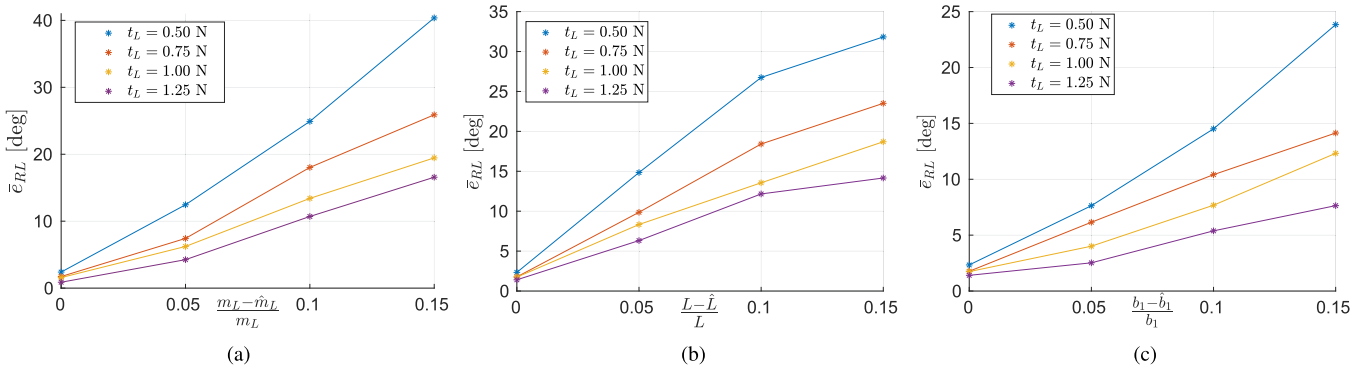

Fig. 6. Each point in the plots is a value of the average attitude error at steady state in a simulation with t_L as indicated in the legend, and parametric uncertainty as indicated in the x-axis of the corresponding plot. A total of 40 simulation results are known in these plots. (a) $\Delta_m \neq 0$. (b) $\Delta_\ell \neq 0$. (c) $\Delta_b \neq 0$.

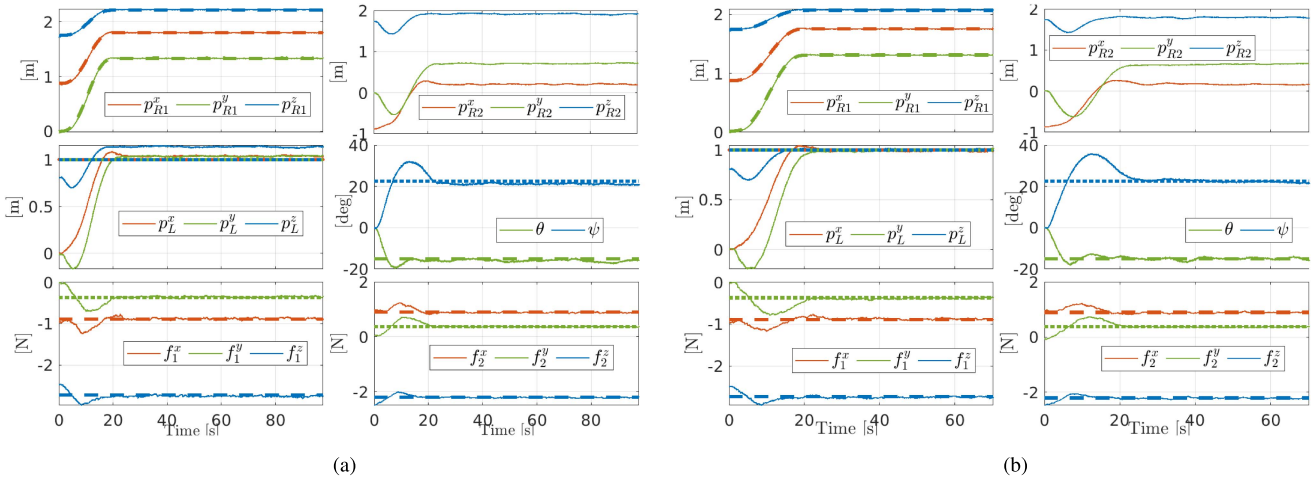

Fig. 7. Simulations for cable parameter uncertainties and $t_L = 1$N. Dotted lines of the same color indicate the corresponding desired quantities. (a) $\hat{l}_{01} = 1.15 \cdot l_{01}$. As expected, $\boldsymbol{p}_L^{\text{eq}} \neq \bar{\boldsymbol{p}}_L$, but $\psi^{\text{eq}} = \bar{\psi}$ and $\theta^{\text{eq}} = \bar{\theta}$. (b) $\hat{l}_{02} = 1.15 \cdot l_{02}$. As expected, $q_L = \bar{q}_L$ at the equilibrium.

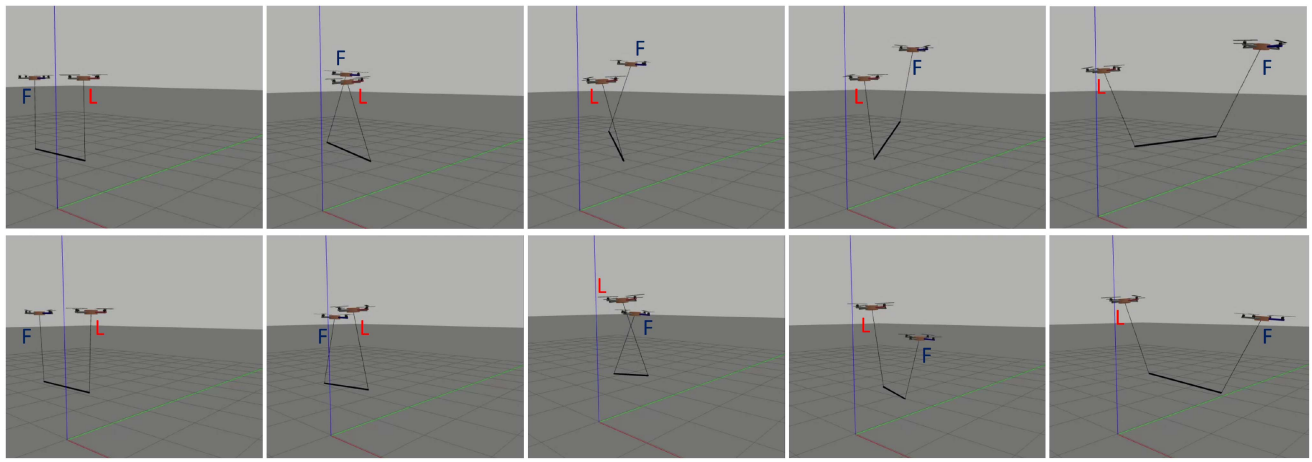

Fig. 8. Two simulated scenarios for $t_L < 0$. Top: $\xi < 0$. Bottom: $\xi > 0$. "L" indicates the leader and "F" the follower.

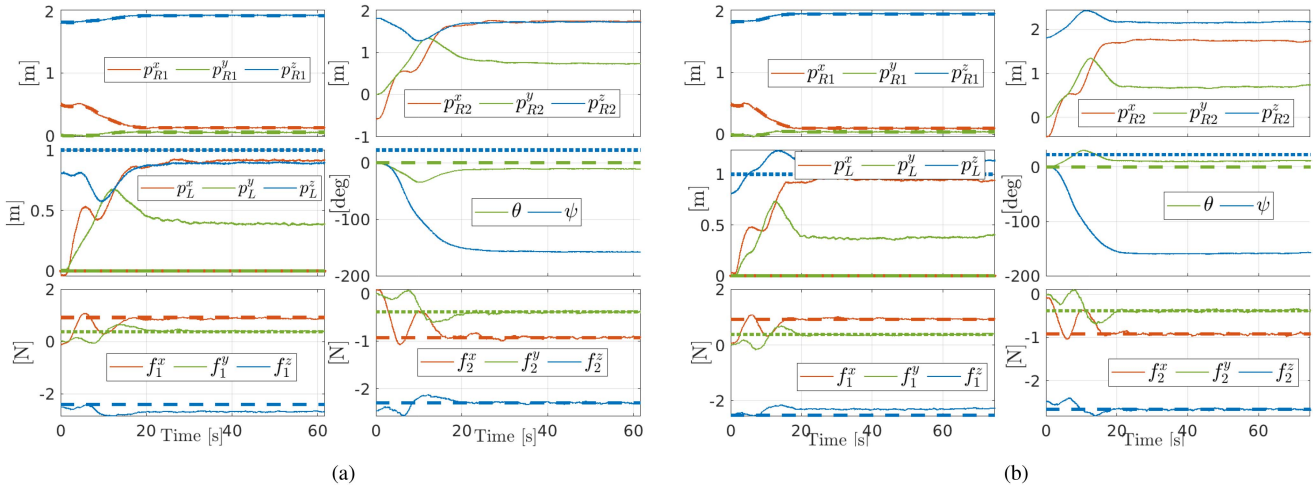

(a) (b)

Fig. 9. Simulations for cable parameter uncertainties and $t_L = -1$N. Dotted lines of the same color are the corresponding desired quantities. (a) $\xi > 0$: $\hat{m}_L = 0.95 m_L$, $\hat{L} = 1.05 L$. (b) $\xi < 0$: $\hat{m}_L = 1.05 m_L$, $\hat{L} = 0.95 L$.

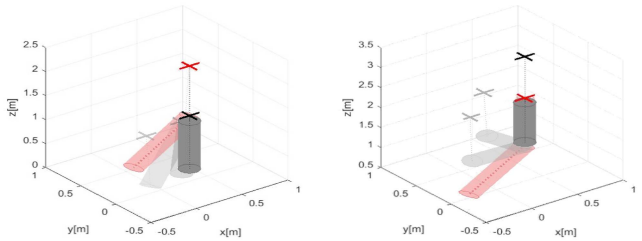

(a) (b)

Fig. 10. Different instants of simulations with $\xi \neq 0$ and $t_L = 0$. The gray cylinder is the load, and the red cross the leader robot. The final pose is solid. The desired (equal to the initial) load is in red. (a) $\xi > 0$. (b) $\xi < 0$.

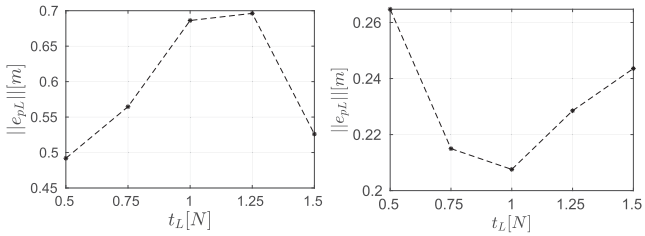

(a) (b)

Fig. 11. $\|\boldsymbol{e}_{pL}\|$ for different values of t_L in two cases in which different values of the uncertainties are considered on two parameters, m and l_{01}. $\boldsymbol{e}_{pL}$ does not always decrease when t_L increases. (a) $\frac{\hat{m}}{m} = 0.85$, $\frac{\hat{l}_{01}}{l_{01}} = 0.9$. (b) $\frac{\hat{m}}{m} = 0.85$, $\frac{\hat{l}_{01}}{l_{01}} = 1.2$.

shows the evolution of the main quantities during the simulated tasks.

D. Case of $t_L = 0$

When it comes to the case in which $\xi \neq 0$ and $t_L = 0$, clearly, the sole equilibrium configurations are not really attainable: all elements of the system are supposed to be aligned vertically, one on top of the others [see Fig. 3(a)]. When simulating such condition in Gazebo, we found that numerical issues arise as the system approaches the expected configuration in which the link that models the load and those that model the cables are vertically aligned. Despite the practical irrelevance of the considered case, with the objective of demonstrating the validity of the theoretical results, simulations have been carried out also for this case, using the MATLAB-Simulink simulator used in [33]. In that simulator, the cables are massless extensible elements, and the force is directly retrieved by the model of the cable without resorting to a wrench observer. Nevertheless, underactuated quadrotors are still considered, as well as the same trajectory controller. The results of two simulations are in Fig. 10. Even though the load has been initialized in the desired configuration, with position $\bar{\boldsymbol{p}}_L = [0\ 0\ 1]^\top$ and the same desired yaw and pitch as before, it moves to the vertical equilibrium, with the leader on top when $\xi > 0$, and the follower on top when $\xi < 0$, as explained by the stability analysis in Section IV.

E. Position Error

First, in Fig. 11, we provide two examples of the different behavior of $\boldsymbol{e}_{pL}$ when t_L increases and different values of the uncertainties are present. This fully supports the finding that the load position error at the equilibrium does not necessarily decrease when t_L is increased.

Anyway, as we have seen from the theory, it is possible to correct the error of the load position by acting solely on the leader robot reference position. This, in turn, does not affect the regulation of the load attitude. In Fig. 12, we report the results of a Gazebo simulation in which the initial and desired load pose are as in Section VI-A, $t_L = 1$ N, and an error equal to 5% of the nominal value is considered on each uncertain parameter. After 41 s, the leader robot corrects its reference position based on the position of the load according to (43). The results show that, consequently, the load is steered to the desired position when the new equilibrium is reached. On the other hand, as expected from the theory [see (10) and (11)], due to the inaccurate knowledge of the system parameters, the value of the pitch angle and the

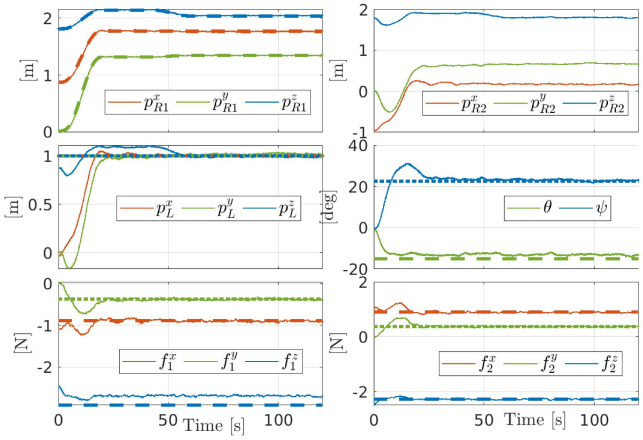

Fig. 12. Simulation results for $t_L = 1$ N and a 5% error on each parameter. Around time = 41 s, signed by a red vertical line, the leader robot reads the load position and corrects its own reference position in order to zero the load position error. Dotted lines of the same color indicate the corresponding desired quantities.

leader robot's cable force at the equilibrium do not match the desired values. Also, as predicted, one can observe in Fig. 12 that their values are not affected by the change in the leader robot position.

VII. Experimental Validation

A. Hardware

The system is made of a 2 m long carbon fiber bar carried by two UAVs by means of two cables that connect the robots at the bar's end. Each cable is 1 m long, the bar weighs 0.300 kg, and each UAV weighs 1.03 kg. The cable anchoring points are installed on the robots' underside at a distance $\boldsymbol{d} = [0\ 0\ -d]^\top$ from their CoM, where $d = 0.15$ cm. Such a geometrical configuration changes the process by which the leader reference position $\hat{\bar{\boldsymbol{p}}}_{R1}$ is generated as it is explained in the Appendix. In addition, the aerial vehicles have an onboard PC, four electronic speed controllers that control the propeller speed in closed loop [51], and a flight controller [51].

B. Software

The control architecture runs in part onboard and in part on a desktop PC. A state-of-the-art unscented-Kalman-filter-based state estimation, which fuses Motion Capture measurements at 120 Hz with the IMU measurements at 1 kHz, and a geometric control are carried out as part of the onboard task at 1 kHz. The admittance filter and the wrench observer are implemented in MATLAB/Simulink and run on the desktop PC. Wi-Fi is used for command and data transfer between the desktop PC and the onboard computers at 100 Hz.

A picture taken from the experiments and highlighting the main setup components is shown in Fig. 13.

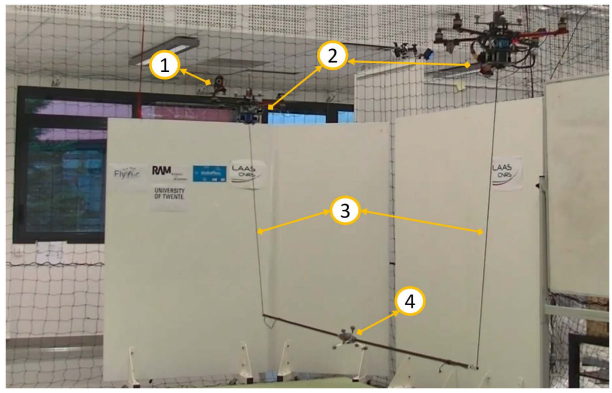

Fig. 13. Picture from the experiment showing: one of the motion capture system cameras: 1) two quadrotors, 2) and two cables, 3) connecting the robots to the carbon fiber load, 4) The markers on the bar track the pose of the object for validation purposes.

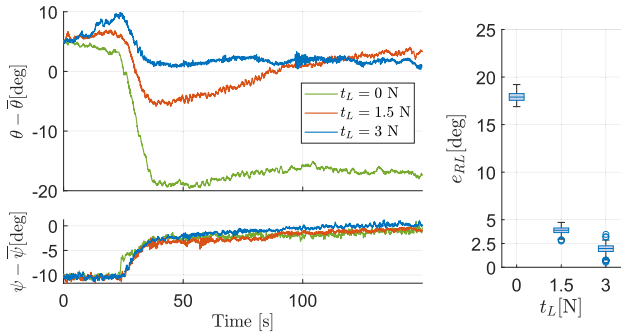

Fig. 14. Evolution of the pitch (top) and yaw (bottom) angle errors during three experiments with no parameter uncertainties for different values of t_L. As expected, the yaw angle converges to the desired value, while for the pitch to do the same, $t_L > 0$ is needed. On the left, the boxplot of the average attitude error over the last 20 s.

C. Experimental Results

Two main sets of experiments were carried out: one in which the controllers use as accurate as possible values of the system parameters, and one in which the controllers use values that differ by 10% from the accurate corresponding value. We refer to the former case as "without uncertainty" and to the latter as "with uncertainty."

For each case, we performed three tests in which the same manipulation task is carried out for three values of t_L, equal to 0, 1.5, and 3 N. The task execution starts with initial steps in which the load, from position $\boldsymbol{p}_L(0) = [0\ 0\ 0]^\top$ m and zero yaw and pitch angles, is lifted by the robots through simple upward motions; hence, the proposed controller is activated, and the robots try to bring the load to $\bar{\boldsymbol{p}}_L = [0.5\ 0\ 1.5]^\top$ m with $\bar{\psi} = 11.5°$ and $\bar{\theta} = -6.9°$.

The case with no uncertainties is depicted in Fig. 14 for all three experiments. The evolution of the attitude error of the load is displayed in the form of quantities $\theta - \bar{\theta}$ and $\psi - \bar{\psi}$. As expected from (18), the yaw angle at the equilibrium coincides with the desired value. Instead, the pitch angle converges to an arbitrary value when $t_L = 0$, in this case with an error around

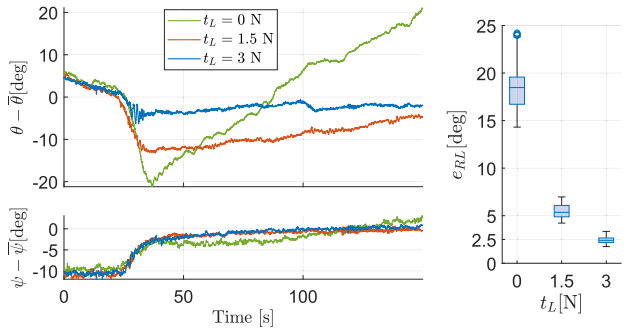

Fig. 15. Evolution of the pitch (top) and yaw (bottom) angle errors during three experiments with 10% uncertainty on each parameter for different values of t_L. As expected, the yaw angle converges to the desired value, while the pitch angle increases for $t_L = 0$ as the load becomes more and more vertical. For $t_L > 0$, the pitch becomes closer and closer to the desired value. On the left is the boxplot of the average attitude error over the last 20 s of the experiments.

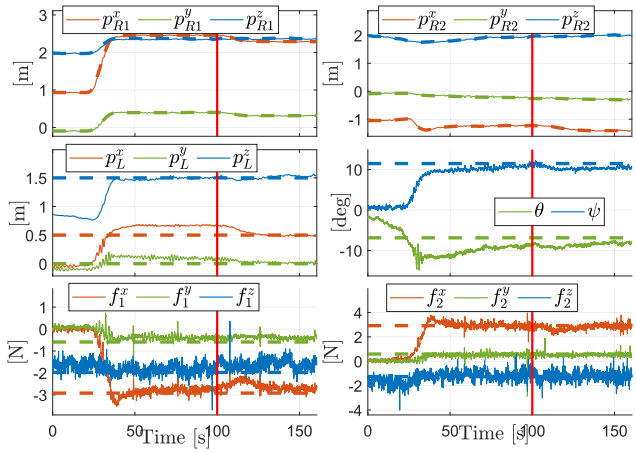

Fig. 16. Experimental results: $t_L = 3$ N and 10% error on each parameter. At time $= 100$ s, signed by a vertical red stripe, the leader robot corrects its reference position to zero the load position error.

18°, when $t_L = 0$. When a positive internal force is applied, the attitude error is reduced up to about 2.5°.

Fig. 15 shows the three tests in the case with uncertainties. Again, in accordance with (18), there is no error on the load yaw angle at the equilibrium. The equilibrium configuration could not be reached with $t_L = 0$. This is also the case in general since it would imply that all bodies are vertically aligned. However, the reader can clearly appreciate the increasing pitch angle evolution, in line with (10). As soon as $t_L > 0$, the pitch angle at the equilibrium approaches the desired value, as expected by (19). Boxplots of the equilibrium error between 130 and 150 s of the task execution are displayed in Figs. 14 and 15 for both the cases, i.e., with and without uncertainties, respectively.

The evolution of all the most relevant quantities can be appreciated in Fig. 16 for another task execution with uncertainties and $t_L = 3$ N. Furthermore, in that experiment, the leader robot corrects its own reference position at time $= 100$ s according to (43), and as a consequence, the load equilibrium position is also adjusted. This validates the load position correction method involving solely the leader robot.

VIII. Conclusion

This article studied the decentralized cooperative manipulation of a cable-suspended load by two aerial robots in the absence of direct communication. The robots were controlled with a leader–follower scheme achieved through an admittance controller on each robot. The controllers made use of system parameters that were subject to uncertainty. The equilibrium points and their stability were formally studied. The theory demonstrated how an internal force that stretches the load longitudinally, generated by nonvertically operated cables, is beneficial in terms of stability of the load pose control as well as robustness to the uncertainties. The theoretical results were validated through numerical simulations and experiments.

In the future, an extension to nonbeam loads with uncertain parameters will be formally addressed. In this case, $N > 2$ robots will be considered as two robots would not be able to control the full pose of the cable-suspended object: rotations around the line connecting the two cables attaching points on the object would not be controlled [52]. Experimental tests outdoors could be valuable to assess the robustness of the method in windy conditions and when relying on outdoor state estimation techniques. Investigating how the approach could benefit from limited communication between the robots, e.g., low-frequency communication, is an interesting future direction. Exploring the possibility of communicationless trajectory tracking and of adaptive laws is left as future work.

Appendix

Underneath the robots, at a distance $\boldsymbol{d}$ from the CoM ($\boldsymbol{d} = [0\ 0\ 0.15]^\top$cm), the cable anchoring points are attached. A reference position for the leader robot taking into account such a displacement is

$$\hat{\bar{\boldsymbol{p}}}^r_{R1} = \hat{\bar{\boldsymbol{p}}}_{R1} - \boldsymbol{R}^r_{R1}\boldsymbol{d} \tag{46}$$

where $\boldsymbol{R}^r_{R1}$ is the leader robot rotational matrix at the equilibrium. This matrix is computed from the leader robot's equilibrium condition under the assumption that the thrust is aligned with the external forces

$$\boldsymbol{R}^r_{R1}\boldsymbol{e}_3 = \frac{m_R g \boldsymbol{e}_3 + \hat{\bar{\boldsymbol{f}}}1}{||m_R g \boldsymbol{e}_3 + \hat{\bar{\boldsymbol{f}}}1||} := \begin{bmatrix} A1 \\ A2 \\ A3 \end{bmatrix}.$$

Assuming that ψ is controlled to 0, $\boldsymbol{R}^r_{R1} = \boldsymbol{R}_Y(\theta^r_{R1})\boldsymbol{R}_X(\phi^r_{R1})$ with $\theta^r_{R1} = \text{atan}(A1/A3)$ and $\phi^r_{R1} = \text{asin}(-A2)$.

References

[1] A. Ollero, M. Tognon, A. Suárez Fernández-Miranda, D. Lee, and A. Franchi, "Past, present, and future of aerial robotic manipulators," *IEEE Trans. Robot.*, vol. 38, no. 1, pp. 626–645, Feb. 2021.

[2] F. Ruggiero, V. Lippiello, and A. Ollero, "Aerial manipulation: A literature review," *IEEE Robot. Autom. Lett.*, vol. 3, no. 3, pp. 1957–1964, Jul. 2018.

[3] H. B. Khamseh, F. Janabi-Sharifi, and A. Abdessameud, "Aerial manipulation—A literature survey," *Robot. Auton. Syst.*, vol. 107, pp. 221–235, 2018.

[4] M. Tognon and A. Franchi, *Theory and Applications for Control of Aerial Robots in Physical Interaction Through Tethers*, vol. 140. New York, NY, USA: Springer, 2020.

[5] M. Tognon, B. Yüksel, G. Buondonno, and A. Franchi, "Dynamic decentralized control for protocentric aerial manipulators," in *Proc. IEEE Int. Conf. Robot. Autom.*, Singapore, 2017, pp. 6375–6380.

[6] G. Skorobogatov, C. Barrado, and E. Salamí, "Multiple UAV systems: A survey," *Unmanned Syst.*, vol. 8, no. 2, pp. 149–169, 2020.

[7] I. Maza, K. Kondak, M. Bernard, and A. Ollero, "Multi-UAV cooperation and control for load transportation and deployment," *J. Intell. Robot. Syst.*, vol. 57, nos. 1–4, pp. 417–449, 2010.

[8] A. Mohiuddin, T. Tarek, Y. Zweiri, and D. Gan, "A survey of single and multi-UAV aerial manipulation," *Unmanned Syst.*, vol. 8, no. 2, pp. 119–147, 2020.

[9] G. Loianno and V. Kumar, "Cooperative transportation using small quadrotors using monocular vision and inertial sensing," *IEEE Robot. Autom. Lett.*, vol. 3, no. 2, pp. 680–687, Apr. 2018.

[10] H.-N. Nguyen, S. Park, and D. J. Lee, "Aerial tool operation system using quadrotors as rotating thrust generators," in *Proc. IEEE/RSJ Int. Conf. Intell. Robots Syst.*, Hamburg, Germany, 2015, pp. 1285–1291.

[11] R. Ritz and R. D'Andrea, "Carrying a flexible payload with multiple flying vehicles," in *Proc. IEEE/RSJ Int. Conf. Intell. Robots Syst.*, 2013, pp. 3465–3471.

[12] F. Caccavale, G. Giglio, G. Muscio, and F. Pierri, "Cooperative impedance control for multiple UAVs with a robotic arm," in *Proc. IEEE/RSJ Int. Conf. Intell. Robots Syst.*, 2015, pp. 2366–2371.

[13] S. Thapa, H. Bai, and J. Acosta, "Cooperative aerial load transport with force control," *IFAC-PapersOnLine*, vol. 51, no. 12, pp. 38–43, 2018.

[14] K. Sreenath and V. Kumar, "Dynamics, control and planning for cooperative manipulation of payloads suspended by cables from multiple quadrotor robots," in *Proc. Robot.: Sci. Syst. Conf.*, Berlin, Germany, 2013.

[15] C. Masone, H. H. Bülthoff, and P. Stegagno, "Cooperative transportation of a payload using quadrotors: A reconfigurable cable-driven parallel robot," in *Proc. IEEE/RSJ Int. Conf. Intell. Robots Syst.*, 2016, pp. 1623–1630.

[16] M. Manubens, D. Devaurs, L. Ros, and J. Cortés, "Motion planning for 6-D manipulation with aerial towed-cable systems," in *Proc. Robot.: Sci. Syst. Conf.*, Berlin, Germany, 2013, p. 8.

[17] A. Mohiuddin, Y. Zweiri, T. Taha, and D. Gan, "Energy distribution in dual-UAV collaborative transportation through load sharing," *J. Mech. Robot.*, pp. 1–14, 2020, doi: 10.1115/1.4046912.

[18] T. Lee, "Geometric control of quadrotor UAVs transporting a cable-suspended rigid body," *IEEE Trans. Control Syst. Technol.*, vol. 26, no. 1, pp. 255–264, Jan. 2018.

[19] G. Li, R. Ge, and G. Loianno, "Cooperative transportation of cable suspended payloads with MAVs using monocular vision and inertial sensing," *IEEE Robot. Autom. Lett.*, vol. 6, no. 3, pp. 5316–5323, Jul. 2021.

[20] D. Sanalitro, H. J. Savino, M. Tognon, J. Cortés, and A. Franchi, "Full-pose manipulation control of a cable-suspended load with multiple UAVs under uncertainties," *IEEE Robot. Autom. Lett.*, vol. 5, no. 2, pp. 2185–2191, Apr. 2020.

[21] F. Rossomando et al., "Aerial load transportation with multiple quadrotors based on a kinematic controller and a neural smc dynamic compensation," *J. Intell. Robot. Syst.*, vol. 100, no. 2, pp. 519–530, 2020.

[22] V. Spurny, M. Petrlik, V. Vonasek, and M. Saska, "Cooperative transport of large objects by a pair of unmanned aerial systems using sampling-based motion planning," in *Proc. IEEE 24th Int. Conf. Emerg. Technol. Factory Autom.*, 2019, pp. 955–962.

[23] P. O. Pereira and D. V. Dimarogonas, "Pose stabilization of a bar tethered to two aerial vehicles," *Automatica*, vol. 112, 2020, Art. no. 108695.

[24] R. C. Sundin, P. Roque, and D. V. Dimarogonas, "Decentralized model predictive control for equilibrium-based collaborative UAV bar transportation," in *Proc. IEEE 39th Int. Conf. Robot. Autom.*, 2022, pp. 4915–4921.

[25] A. Tagliabue, M. Kamel, S. Verling, R. Siegwart, and J. Nieto, "Collaborative transportation using MAVs via passive force control," in *Proc. IEEE Int. Conf. Robot. Autom.*, Singapore, 2016, pp. 5766–5773.

[26] M. Gassner, T. Cieslewski, and D. Scaramuzza, "Dynamic collaboration without communication: Vision-based cable-suspended load transport with two quadrotors," in *Proc. IEEE Int. Conf. Robot. Autom.*, Singapore, 2017, pp. 5196–5202.

[27] D. K. D. Villa, A. S. Brandão, R. Carelli, and M. Sarcinelli-Filho, "Cooperative load transportation with two quadrotors using adaptive control," *IEEE Access*, vol. 9, pp. 129148–129160, 2021.

[28] J. Fink, N. Michael, S. Kim, and V. Kumar, "Planning and control for cooperative manipulation and transportation with aerial robots," in *Proc. 14th Int. Symp. Robot. Res.*, Lucerne, Switzerland, 2009, pp. 324–334.

[29] J. Goodman and L. Colombo, "Geometric control of two quadrotors carrying a rigid rod with elastic cables," *J. Nonlinear Sci.*, vol. 32, no. 5, pp. 1–31, 2022.

[30] D. Mellinger, M. Shomin, N. Michael, and V. Kumar, "Cooperative grasping and transport using multiple quadrotors," in *Proc. Int. Symp. Distrib. Auton. Robot. Syst.*, 2013, pp. 545–558.

[31] Z. Wang and M. Schwager, "Force-amplifying N-robot transport system (force-ants) for cooperative planar manipulation without communication," *Int. J. Robot. Res.*, vol. 35, no. 13, pp. 1564–1586, 2016.

[32] A. Tagliabue, M. Kamel, R. Siegwart, and J. Nieto, "Robust collaborative object transportation using multiple MAVs," *Int. J. Robot. Res.*, vol. 38, no. 9, pp. 1020–1044, 2019.

[33] M. Tognon, C. Gabellieri, L. Pallottino, and A. Franchi, "Aerial co-manipulation with cables: The role of internal force for equilibria, stability, and passivity," *IEEE Robot. Autom. Lett.*, vol. 3, no. 3, pp. 2577–2583, Jul. 2018.

[34] C. Gabellieri, M. Tognon, D. Sanalitro, L. Pallottino, and A. Franchi, "A study on force-based collaboration in swarms," *Swarm Intell.*, vol. 14, no. 1, pp. 57–82, 2020.

[35] H. Lee, H. Kim, and H. J. Kim, "Planning and control for collision-free cooperative aerial transportation," *IEEE Trans. Autom. Sci. Eng.*, vol. 15, no. 1, pp. 189–201, Jan. 2018.

[36] H. Lee, H. Kim, W. Kim, and H. J. Kim, "An integrated framework for cooperative aerial manipulators in unknown environments," *IEEE Robot. Autom. Lett.*, vol. 3, no. 3, pp. 2307–2314, Jul. 2018.

[37] S. Thapa, H. Bai, and J. Á. Acosta, "Cooperative aerial manipulation with decentralized adaptive force-consensus control," *J. Intell. Robot. Syst.*, vol. 97, no. 1, pp. 171–183, 2020.

[38] A. Bicchi, "On the problem of decomposing grasp and manipulation forces in multiple whole-limb manipulation," *Robot. Auton. Syst.*, vol. 13, no. 2, pp. 127–147, 1994.

[39] M. Kamel, T. Stastny, K. Alexis, and R. Siegwart, "Model predictive control for trajectory tracking of unmanned aerial vehicles using robot operating system," in *Robot Operating System (ROS)*, Berlin, Germany: Springer, 2017, pp. 3–39.

[40] M. Ryll, D. Bicego, and A. Franchi, "Modeling and control of FAST-Hex: A fully-actuated by synchronized-tilting hexarotor," in *Proc. IEEE/RSJ Int. Conf. Intell. Robots Syst.*, Daejeon, South Korea, 2016, pp. 1689–1694.

[41] K. Nonami, F. Kendoul, S. Suzuki, W. Wang, and D. Nakazawa, *Autonomous Flying Robots: Unmanned Aerial Vehicles and Micro Aerial Vehicles*. Berlin, Germany: Springer, 2010, ch. 12.

[42] J. R. Goodman, J. S. Cely, T. Beckers, and L. J. Colombo, "Geometric control for load transportation with quadrotor UAVs by elastic cables," 2021, *arXiv:2111.00777*.

[43] C. Bisig, J. B. Montejo, M. R. Verbryke, A. Sathyan, and O. Ma, "Genetic fuzzy systems for decentralized, multi-UAV cargo handling," in *Proc. AIAA Scitech Forum*, 2020, Art. no. 1117.

[44] A. Yiğit, M. A. Perozo, L. Cuvillon, S. Durand, and J. Gangloff, "Novel omnidirectional aerial manipulator with elastic suspension: Dynamic control and experimental performance assessment," *IEEE Robot. Autom. Lett.*, vol. 6, no. 2, pp. 612–619, Apr. 2021.

[45] M. Ryll et al., "6D physical interaction with a fully actuated aerial robot," in *Proc. IEEE Int. Conf. Robot. Autom.*, Singapore, 2017, pp. 5190–5195.

[46] R. Horst, P. M. Pardalos, and N. V. Thoai, *Introduction to Global Optimization*. Springer, 2000.

[47] H. K. Khalil and J. W. Grizzle, *Nonlinear Systems*, vol. 3. Upper Saddle River, NJ, USA: Prentice-Hall, 2002.

[48] A. S. Aghdam, M. B. Menhaj, F. Barazandeh, and F. Abdollahi, "Cooperative load transport with movable load center of mass using multiple quadrotor UAVs," in *Proc. IEEE 4th Int. Conf. Control, Instrum., Autom.*, 2016, pp. 23–27.

[49] T. Lee, M. Leoky, and N. H. McClamroch, "Geometric tracking control of a quadrotor UAV on SE(3)," in *Proc. IEEE 49th Conf. Decis. Control*, Atlanta, GA, USA, 2010, pp. 5420–5425.

[50] M. Ryll et al., "6D interaction control with aerial robots: The flying end-effector paradigm," *Int. J. Robot. Res.*, vol. 38, no. 9, pp. 1045–1062, 2019.

[51] A. Franchi and A. Mallet, "Adaptive closed-loop speed control of BLDC motors with applications to multi-rotor aerial vehicles," in *Proc. IEEE Int. Conf. Robot. Autom.*, Singapore, 2017, pp. 5203–5208.

[52] N. Michael, J. Fink, and V. Kumar, "Cooperative manipulation and transportation with aerial robots," *Auton. Robots*, vol. 30, no. 1, pp. 73–86, 2011.

Chiara Gabellieri (Member) received the B.Sc. degree in bioengineering, the M.Sc. (Hons.) degree in robotics and automation engineering, and the Ph.D. degree in information engineering from the University of Pisa, Pisa, Italy, in 2014, 2017, and 2021, respectively.

She is currently a Researcher with the Robotics and Mechatronics Group, University of Twente, Enschede, The Netherlands. She received the Marie Skłodowska-Curie postdoctoral fellowship with the Flyflic project in 2022. She leads a Work Package in the European coordination and support project AeroSTREAM. She was with the Laboratory for Analysis and Architecture of Systems, French National Center for Scientific Research, University of Toulouse, Toulouse, France, from 2017 to 2018 and a visiting Ph.D. student with the German Aerospace Center, Oberpfaffenhofen, Germany, from 2019 to 2020. Her current research interests include environmental robotics and aerial manipulation.

Dr. Gabellieri was an Associate Editor for International Conference on Robotics and Automation in 2022 and 2023 and for IEEE/RSJ International Conference on Intelligent Robots and Systems in 2023.

Marco Tognon (Member) received the M.Sc. degree in automation engineering from the University of Padua, Italy, in 2014, and the Ph.D. degree in robotics from INSA Toulouse, Toulouse, France, in 2018.

Since November 2022, he has been a tenured Researcher with in the Rainbow Team, INRIA, Rennes University, Rennes, France. Before this, he was a Postdoctoral Researcher with the Autonomous System Lab, ETH Zurich, Zurich, Switzerland. His master's thesis was carried out at MPI for Biological Cybernetics, Tübingen, Germany. He developed his doctoral thesis with the Laboratory for Analysis and Architecture of Systems, French National Center for Scientific Research, University of Toulouse, Toulouse, France, where he was a Postdoctoral Researcher from 2018 to 2020. His current research interests include robotics, aerial physical interaction, multirobot systems, and human–robot physical interaction.

Dr. Tognon was an Associate Editor for IEEE International Conference on Robotics and Automation and IEEE/RSJ International Conference on Intelligent Robots and Systems for the years 2019–2020 and an Area Chair for 2023 Robotics: Science and Systems Conference. He received three prizes for his doctoral thesis.

Dario Sanalitro (Member) received the M.Sc. degree in automation engineering and control of complex systems from the University of Catania, Catania, Italy, in 2017, and the Ph.D. degree in robotics from the National Institute for Applied Sciences, Toulouse, France, in 2022.

He was a Postdoctoral Researcher with the Laboratory for Analysis and Architecture of Systems, French National Center for Scientific Research, University of Toulouse, Toulouse, France, in 2022. He is currently an Assistant Professor with the University of Catania, Catania, Italy. His research interests include robotics, aerial physical interactions, and multirobot systems.

Antonio Franchi (Fellow) received the Ph.D. degree in system engineering from the Sapienza University of Rome, Rome, Italy in 2010, and the HDR degree in science from the National Polytechnic Institute of Toulouse, Toulouse, France, in 2016.

From 2014 to 2019, he was a tenured Researcher with Laboratory for Analysis and Architecture of Systems, French National Center for Scientific Research, University of Toulouse, Toulouse, France. From 2019 to 2021, he was an Associate Professor with the Robotics and Mechatronics Group, University of Twente, Enschede, The Netherlands, where he has been a Full Professor in Aerial Robotics Control since 2022. Since 2023, he has also been a Full Professor with the Department of Computer, Control and Management Engineering, Sapienza University of Rome. He coauthored more than 160 publications in peer-reviewed international journals, books, and conferences. His research interests include design, control, and estimation for robotic systems applied to multirobot systems and aerial robots.